General comments

We would like to thank the three reviewers for their insightful comments that helped to greatly improve this work. The manuscript was modified to address the requests from the reviewers, while keeping the original objectives of the work.

Matthew Johnson was added to the co-authors list to give him credit for providing information that allowed to conduct measurements during the case studies shown in this work. He also provided insightful comments on the WRF-Chem/WACCM/lidar intercomparison and results.

Reviewer #1

General comments

The analysis is thorough and compelling, but I think the authors should also use measurements from the extensive network of ozone monitors in the Los Angeles area to provide more context for their results. This would better link these mountaintop measurements to the issue of regional ozone attainment they invoke in both the introduction and conclusions.

Thanks for the useful comments. We decided to include supporting information from nearby stations (see also reviewer #2 answers regarding the shift in the ozone maxima, observed at TMF but not at Phelan and Crestline stations) in the surface ozone discussion as well as in the case studies.

Additional comments

P2, L46. ". . .near-surface measurements carried out at. . ."

Done

P3, L63. ". . .northwest of Wrightwood..", "The site hosts. . ."

Done

P3, L64-67. It is never clearly stated that the Chen study was based on DOAS. Perhaps start with "Differential Optical Absorption Spectroscopy (DOAS) measurements by Chen et al. . ."

Done

P3, L67. "Similar conclusions have been reached. . ."

Done

P4, Table 1. Is the temporal resolution of the TMTOL really 1 hour or is that just the integration time used for the comparisons?

1 hour is the integration time. The data acquisition resolution is 3 min, but only very noisy datasets can be obtained with the resolution.

In order to clarify this, "1 hour" was replaced by "1-hour averaging".

P4, L86 and Figure 2. Is there an explanation for why the TMTOL values are consistently higher than the UAV values below 75 ppb? Did the UAV carry a standard ECC ozonesonde? Also, what is the relevance of showing the "Days since first validation"? Is this meant to somehow account for the one outlier?

At this time, we have no explanation for this difference, but it is consistent with the agreement observed in the cited paper (Leblanc et al., 2018). The higher values of TMTOL could be related to aerosol extinction effects, but since no systematic study was conducted to determine this, we decided to take it out from the paper.

The idea behind showing the time difference is to provide evidence that the receiver is stable over time. Since the lowest altitudes of the lidar retrieval are very sensitive to misalignment, showing little change over time provides additional confidence regarding the stability of the receiver.

The following clarifications were introduced:

"with an UAV-borne ozonesonde" -> "with an UAV-borne electrochemical concentration cell (ECC) ozonesonde"

"performance" -> "performance over time".

P7, L164. Would the authors care to comment on the clear seasonal shift between 2012-2014 (highest O3 in May and June) and 2017-2020 (highest O3 in July and August) in Figure 3a?

The reason for this shift is unclear. The low number of years used here do not allow firm conclusions on the role of interannual variability, which is partly driven by year-to-year changes in meteorology and regional and local wildfire activity. Given the degree of uncertainty associated with this feature, we are not able to comment on it.

P8, L181 and Figure 4. Are the seasons defined here as Fall (SSO), W(DJF), Sp(MAM), and Summer (JJA) or by equinox/solstice?

We use the meteorological definition of seasons on the paper. Fall (SON), Winter (DJF), Spring (MAM) and Summer (JJA).

The following clarification was introduced:

"Here, summer, fall, winter and spring are defined as June-July-August (JJA), September-October-November (SON), December-January-February (DJF), and March-April-May (MAM) respectively."

P8, L183 and below. "forecast" is the preferred form of the verb-not "forecasted".

Done.

P8, L186. Are the shifts in wind direction consistent with the lower resolution of the model topography?

Unfortunately, since TMF is surrounded by complex terrain, it is not possible to determine the exact impact of the lower resolution topography without re-running the model at a much higher resolution. While this could be an interesting study, it is out of the scope of this work.

P8, L195. What was the resolution of the meteorology used for the HYSPLIT back trajectories?

The HYSPLIT trajectories were calculated based on the WRF-Chem met fields (12x12 km). See Sec. 2.5 for more details.

The following clarification was introduced:

"back-trajectories for summer 2019 and summer 2020" -> "back-trajectories based on WRF-Chem meteorological fields for summer 2019 and summer 2020"

P8, L206. "The trajectories corresponding to the 210-240◦ prevailing winds. . ."

"to the prevailing winds end over this high surface" replaced by "to the prevailing winds (210-240 degrees) end over this high surface"

P8, L207. ". . .with respect to the 250-300◦ back trajectories. . ."

Done

P9, Figures 3b-3d. These plots are confusing. What statistics are represented by the box-and-whisker plots? I assume the shading refers to 2019 and 2020, but this is not explicitly stated. What do the dark gray diamonds represent? By the way, the plotted symbols are time series and not "scatter plots".

Shading refers to 2019 and 2020 as in Figure 3a. The box plot provides the quartile distribution of the WACCM stratospheric ozone, temperature and humidity for each month. The single black diamonds represent values out of the 1.5*interquartile range (IQR), also called 'outliers' in this kind of plots. The light and dark orange points are the values that these variables (WACCM stratospheric ozone, humidity and temperature) took during each exceedance day in 2019-2020. The idea behind the plot is to show how far out of the norm the ozone exceedance days are with respect to these variables and indicate whether stratospheric ozone had a role on the exceedances.

In order to clarify these points, we added a legend to panel Figure 3b showing that colors refer to 2019-2020 and added the following sentence to the figure caption:

Values exceeding 1.5 times the interquartile range (whiskers) are also shown (black diamonds).

And replaced

''are shown as scatter plots" -> "are shown for comparison (dots)"

P11, L211. The discussion here skips back from Figures 5 and 6 to Figure 4 without warning. It took me a while to figure out the authors were referring to Figure 4 in the paragraph that followed. Perhaps revise to "During summer 2019, PM10 observations and forecast (third and sixth rows of Figure 4). . .".

Done

P11, L213. "A difference is observed for ENE. . ."

Done

P11, L229. ". . .focused on the free troposphere. . ."

Done

P11, L214. Were there any significant wildfire influences in the Fall of 2019?

No significative wildfire influences were registered during this period of study.

P11, L217. The Met One 212 has a lower size cut at 0.3 µm and thus may be excluding the smaller particles in the model analysis.

While the lower size cut at 0.3 um diameter will certainly have some impact on the PM10 retrieval, the influence is expected to be less than 10% due to the r^3 dependency of the aerosol volume/mass distribution. For example, for a typical volume size distribution derived from AERONET at TMF, only a small fraction of the volume size distribution falls under 0.15 um radius:

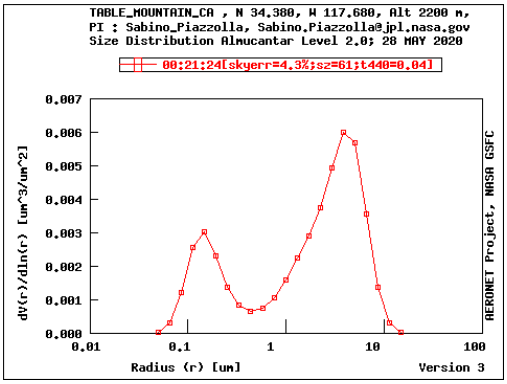

The following clarification was added to the manuscript:

"Since the cut-off diameter of the particle counter is 0.3 um, an underestimation in the derived PM10 values is expected for fine-mode dominated aerosol events"

P12, 13. Figures 5 and 6. The gray back trajectories are hard to see in some of the plots. Perhaps use heavier white or magenta lines?

Lines were change to white (with black borders) to improve visibility.

P16, L279+. In my opinion, it would be better to switch sections 4.1 and 4.2 and describe the pollution transport event first since this is the more typical event. That would help to put the TMTOL and ceilometer measurements from Figure 9 in better context.

Done.

P16, L284. This sentence is awkward and could perhaps be phrased better.

Done. The sentence was rephrased and simplified.

"*Additionally, and although WRF-Chem and WACCM forecasted enhanced ozone in the lower free troposphere associated with a SI, WRF-Chem did not forecast an effect on the surface ozone as it finally occurred, which illustrates the challenges associated with modeling the entrainment into the nocturnal surface layer and in complex terrain.*"

Was changed to:

"*Additionally, this case study illustrates the challenges of forecasting the impact of SIs on surface ozone concentration. In particular, the difficulties associated with an accurate representation of the entrainment into the nocturnal surface layer in complex terrain.*"

P17, L295. The WRF-Chem RH isn't shown.

Added as vertical profiles for three different times in Fig. 13.

P18, F9 caption. (a) The CO scale is missing. (b) Please note that the PBL height is from the ceilometer measurements in (c). The ozonesonde profile mentioned in the caption does not appear to be in the plot. (d) The plot is already complicated, but it would be useful to see the WRF-Chem RH since it is mentioned in the text.

The following changes were introduced: (a) Labels for CO (10,20 and 30 ppb) were added to the plots.

The ozonesonde corresponds to the second case study. This was corrected by changing the ozonesonde phrase from the Figure 9 caption to the Figure 11 caption.

The WRF-Chem RH was added as a separate plot for three different times, together with ozone and potential temperature to illustrate the reasons why WRF-Chem didn't capture an increase in the surface ozone associated with the stratospheric intrusion.

P19, L340. Again, it would be useful if the TMF surface measurements were compared with the regulatory measurements, particularly those from particularly Phelan and Crestline.

We added the following to the end of Sec. 4.1:

"*The surrounding Phelan and Crestline stations exhibited an opposite behavior to TMF, with the surface ozone greatly exceeding the EPA threshold and measurements showing generally higher ozone than forecast (Fig. A2).*"

And added a figure to the appendix:

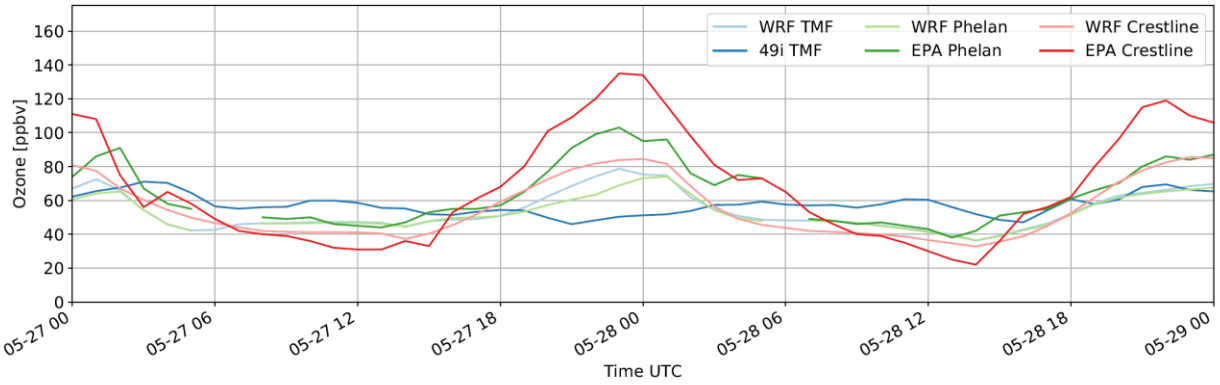

Figure A2. Forecast and measured surface ozone concentration at TMF and nearby stations (Phelan and Crestline) for the period comprehended between 27-28 May 2020.

P21, L357. ". . .the closest time to the ozonesonde. . ."

Done.

P23, L281. The high aerosol content of the irruption is not obvious from the ceilometer measurements.

An indicator ('See text') was added to Fig. 15c.

P24, L396. This case can be contrasted with that described in Langford et al 2012* where the descent of a deep SI also caused surface O3 to decrease in the Los Angeles Basin. In that case, however, the surface RH also decreased as drier air from aloft displaced local pollution.

The following paragraph and appendix figure were added:

"The ozone monitoring station in central LA (Fig. 3A) did not record any obvious increase in surface ozone associated with any of the two SI events. For the second SI event, the ozone concentration actually dropped more abruptly than forecast, likely related to the onset of the cold front and associated reduced photochemical activity. The Crestline surface monitoring station (the closest high-elevation site to TMF) did show an episodic increase in surface ozone concentrations a few hours before the increase observed at TMF. Surface ozone forecast at the surrounding stations followed the general trend of the observations, but failed to reproduce the SI related increases at the TMF and Crestline station; likely as a result of insufficient entrainment into the nocturnal surface layer. These episodes resemble a case study presented in Langford et al. (2012), where another deep SI was determined to be responsible for an ozone threshold exceedance at the Joshua Tree National Park during 28 May 2010, while the rest of the stations in the LA basin showed a decrease in the ozone concentration as a result of decreased photochemical activity associated with the passage of a cold front."

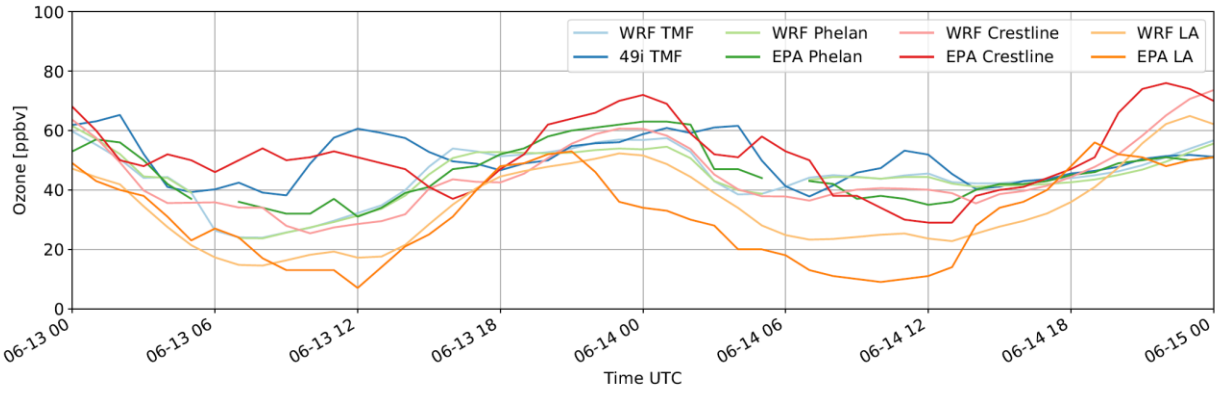

Figure A3. Forecast and measured surface ozone concentration at TMF and nearby stations (Phelan, Crestline and LA) for the period comprehended between 13-15 June 2020.

P24, L406. "This result,. . ."

Done.

Reviewer #2

General comments

The manuscript submitted by F. Chouza and co-authors concerns the analysis of ozone measurements at the Table Mountain (TMO) California station. The objectives are multiple (1) to demonstrate the contribution of new measurements at low altitudes of the TMO lidar for the analysis of regional

pollution (2) to analyze the respective role of stratospheric intrusions and regional pollution on ozone threshold exceedances (3) an evaluation of the performance of WRF-CHEM model ozone forecast for the analysis of pollution episodes.

The paper contains many interesting results based on a joint analysis of observation and modeling. It certainly deserves a publication in ACP. My main criticism will be on the readability of the objectives and the overall coherence of the paper. The authors are probably trying to meet too many objectives in the same paper. The evaluation of the WRF CHEM forecast seems to be both the most original objective considering the previous publications on the analysis of ozone measurements in the Los Angeles area and a good approach to ensure consistency in the paper. This could be improved by (1) a better presentation of the objectives in the introduction (2) add a discussion of model/measurement differences in section 3.1, otherwise the results presented will be difficult to use (3) Focus section 4 on the evaluation of model performance for the three case studies. The latter could be seen as examples to discuss the differences identified in section 3.2 using the 726 lidar profiles. Indeed the identification of the 3 high surface O3 drivers at TMF based on section 4 is not really new (see previous papers by Cooper, Langford, Lin) and the same results could be very useful if the discussions focus on the model forecast performances to represent theses processes.

Many thanks for the valuable comments on the general structure of the paper. The introduction was modified as suggested in order to clarify the objectives of this work. Additional comments and comparisons with the models were added to emphasize that aspect of the paper.

Detailed remarks

Line 37 and 51: Relevant objectives are provided here and the introduction generally misses a list of these objectives in addition to the list of tools used.

The paragraph between L44-52 was modified to include the list of paper objective together with the tools used to address them. The new paragraph is:

"In this work, surface and lidar measurements conducted at the Jet Propulsion Laboratory Table Mountain Facility (JPL TMF) in the San Gabriel Mountains (Southern California) are used to address three main objectives. Firstly, to demonstrate the new near-range measurement capabilities of the Table Mountain tropospheric ozone lidar and their value for pollution transport and deep stratospheric intrusion studies. Secondly, to investigate the relative impact of regional pollution transport and stratospheric intrusions on the exceedances of the National Ambient Air Quality Standards at TMF, and to determine the representativeness of surface measurements as a proxy for the free troposphere. Finally, to use these surface and vertical profiles to evaluate the performance in complex terrain of the Weather Research and Forecasting model coupled with Chemistry (WRF-Chem) and Whole Atmosphere Community Climate Model (WACCM) forecasts produced daily by the Atmospheric Chemistry Observations and Modeling (ACOM) laboratory at the National Center for Atmospheric Research Atmospheric (NCAR)."

And slightly modified the following paragraph (paper structure) to emphasize the last two objectives (SI/pollution impact and model performance) :

"Section 3 presents an analysis of the relative impacts of pollution transport and stratospheric intrusions to the observed ozone threshold exceedances at TMF, as well as an evaluation of the WRF-Chem forecast based on ground and vertical profile measurements conducted between May 2019 and September 2020

(the period during which the model data is available). In section 4, three case studies depicting the main mechanisms driving high surface ozone events at JPL TMF are discussed and compared with the WRF-Chem/WACCM forecast of these events."

Line 40-44: While the representativity of a mountain top station to characterize PBL or free tropospheric air is a very important point, it is not clear how the paper address this question in section 3.1 or in section 4. If some results address this question they should be mentioned in section 3 or 4.

Part of this question is addressed in Fig. 3 and the associated discussion. Generally speaking, the large number of ozone threshold exceedances observed at TMF cannot be explained by the influence of stratospheric intrusions and is mainly associated with low level transport from the LA basin area. Considering the strong influence of low-level transport at TMF, it cannot be assumed that the surface measurements at TMF are representative of the free troposphere. In order to provide further evidence of the pollution transport impact, we decided to add a fifth panel to Fig. 3 that shows the WRF-Chem forecasted anthropogenic CO tracer concentrations at TMF as well as the values corresponding to exceedance days.

The following discussion was added towards the end of the subsection:

"Additionally, the concentrations of the anthropogenic CO tracer as forecasted by WRF-Chem appear to be highly variable and generally non-negligible over the whole year, with median values of 12 ppbv during winter and over 25 ppbv during summer, suggesting that surface and near-ground measurements at TMF are strongly influenced by local sources and cannot be generally assumed to be representative of the free troposphere."

Line 175 : Scatter of WACCM stratospheric tracer on O3 exceedance days are a little hard to read in figure 3.b but it seems that the mean is always higher than the median or even than the upper interquartile of the stratospheric tracer for the overall data set. So is it true to say that the stratospheric intrusion plays a limited role based on this unique feature? I am not sure I understand the differences between the black and color dots in Fig. 3. On the other hand it is true to say that the O3 exceedance days with RH>50 % are often observed. So interpretation of the WACCM forecast is not straightforward. May be the age of the stratospheric tracer could help.

Unfortunately, the WACCM product does not include the stratospheric tracer age. Instead, we decided to add anthropogenic CO tracer values from WRF-Chem as discussed in the previous answer.

Line 179 : Make a new section here because there is no obvious link between the analysis of the O3 exceedance days shown in Fig. 3 and the new question discussed in Fig. 4 where the wind and diurnal cycle dependency of surface and model are shown.

A new section was created to separate the pollution/stratospheric influence discussion from the angular dependence discussion. The first subsection was renamed as "*The impact of pollution transport and stratospheric intrusions on high ozone days*", while the second subsection was named "*Surface ozone and PM10 as function of time and wind direction*". Section 3 title was changed from "*WRF-Chem evaluation*" to "*General ozone features and model evaluation*" to account for the discussion beyond the WRF-Chem/WACCM evaluation.

Line 190 : I agree it is a nice result of this study. However one could expect some hints about of the model difficulties to reproduce this diurnal cycle. Is a well known feature or specific to the TMO data set ?

The following paragraph was added to the discussion:

"*A comparison of the WRF-Chem surface ozone output with the nearby surface ozone stations of Phelan and Crestline, suggests that this temporal shift in the ozone maximum is a particular feature of the model over TMF, while the underestimation of the ozone levels during morning hours by WRF-Chem is common to all three stations (Fig. A1). The cause of this localized temporal shift is uncertain at this point, but it might be related to the smoothing of the terrain in the model and its impact on the slope mountain effect.*"

Additionally, Fig. 1 and Fig. 7 were modified to include Phelan and central LA among the relevant stations for this study:

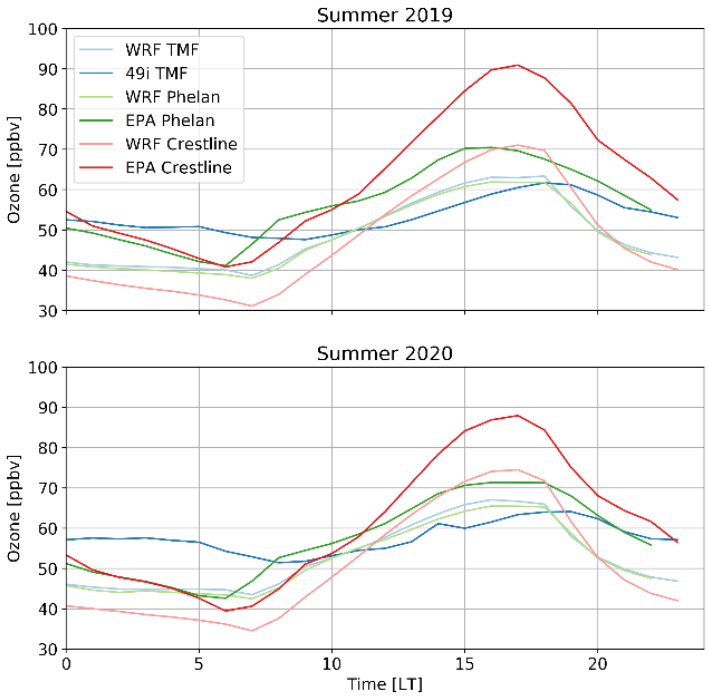

Figure A1. Mean ozone daily cycle at TMF and nearby stations together with the corresponding WRF-Chem output for summer 2019 and summer 2020.

Line 191 -201: The authors give a great importance to the distribution of ozone in the prevailing wind sector but why do you expect an ozone maxima for this sector ? Indeed according to the ozone distribution shown in figure 5, the ozone max are found west and south of TMO. So the TMO surface ozone max is obviously found for the western and southern wind sectors. I propose to simplify the discussion line 191-201 and use Figure 5 to explain why the observed ozone maxima are for the western and southern sectors. Then the second level of discussion is the comparison of the ozone/wind dependency for the observations and the forecast, which is quite good.

The ozone maxima were expected to coincide with the prevailing wind direction because it is approximately coincident with the direction of the highest population areas in the LA basin. Certainly because of the complex relationship between NOx and VOCs, the maximum in emissions might not be coincident with the maximum in the ozone production (as became evident when looking at the WRF-Chem plots). Additionally, it is interesting to note that despite being surrounded by complex terrain, the trajectories are fairly straight and mixing does not blur this angular dependence in the ozone arriving to TMF.

Additionally, as supporting validation information on WRF-Chem and following the comments from reviewer #1, we decided to add the actual values from EPA stations to Figs. 5 and 6.

These modifications were accompanied with the following addition:

"The comparison with the EPA surface ozone monitoring stations (see LA, Santa Clarita, Crestline, and Phelan measurements in Figs. 5a,b and 6a,b) shows a good qualitative agreement with the WRF-Chem output, but with measurements showing generally higher ozone levels at Crestline/Santa Clarita and lower values at the central LA site. The latter can be attributed to enhanced near-surface titration associated with high surface NO_x levels (Figs. 5c,d and 6c,d)."

Figure 5 : add TMO position on this figure, trajectories are also hard to read and it is not clear why they are different for top, middle and bottom panel

The TMF position was added to the figure. Based on this and reviewer #1 comments, we decided to change the color of the trajectories to white (with black borders) to enhance the contrast. Regarding the three rows of panels, the trajectories are the same for all of them. Panels (a), (c) and (e) show the same trajectories (westerly wind), while (b), (d) and (f) show also the same trajectories (prevailing winds).

Section 3.1 A summary about the main findings about this surface measurement/model comparison must be given at the end of the section: accuracy of model ozone field around TMO, biais in diurnal variation, accuracy of ozone titration in the model.

The following paragraph was added at the end of the section to summarize the main findings of the measurement/model comparison as well as regarding the influence of pollution transport on the summer surface ozone levels at TMF.

"WRF-Chem was shown to be able to qualitatively reproduce most of the features observed in the spatio-temporal distributions of ozone and PM10 at TMF and the surrounding stations. Some differences were observed regarding the amplitude of the ozone diurnal cycle at TMF and the nearby stations (Figs. 4 and S1). In the particular case of TMF, the forecasted maximum of the ozone diurnal cycle was about 3 hours earlier than the measured maximum. As also shown in Sec. 3.1, the results shown in this subsection indicate that surface ozone concentrations during summer at TMF are strongly influenced by pollution transport from the LA basin region. Transport from central LA, where titration limits the surface ozone concentrations, is characterized by generally lower ozone levels at TMF, while transport from Santa Clarita is generally associated with higher ozone concentrations."

Section 3.2 It is a very interesting section and there is little published work where many lidar profiles are statistically compared with regional-scale CTM simulations. However the discussion is not very developed and the lidar vertical resolution is probably not the main driving factor. While large

differences due to small time or spatial shift of the simulated ozone layers above TMO are expected near the tropopause or at the PBL top, it is unexpected to find 30-50 % differences at 7.5 km. A small discussion about possible reason for this overestimate of the forecast could be added. Was this feature already observed during model evaluation in the free troposphere ? Is it specific to TMO and why ? The differences seems also worse during nighttime (except in summer 2020) while the lidar accuracy is less for daytime observations. Do you have an explanation for this ?

The WRF-Chem runs are initialized using WACCM. We ran a comparison of the lidar measurements with WACCM and we observed the same difference, suggesting that the problem comes from WACCM. The following was added to the section:

"The observed variability in the free troposphere also shows a clear seasonal dependence, with larger variability during summer and reduced variability during winter. The same seasonal pattern is also visible in the WRF-Chem profiles.

The WACCM forecast shows a very similar behavior to the one described for WRF-Chem, including the altitude-dependent bias. Since the WRF-Chem chemical boundary conditions are determined by the WACCM forecast (Sec. 2.5), the bias observed in the WRF-Chem runs is likely a result of the bias in the WACCM forecast."

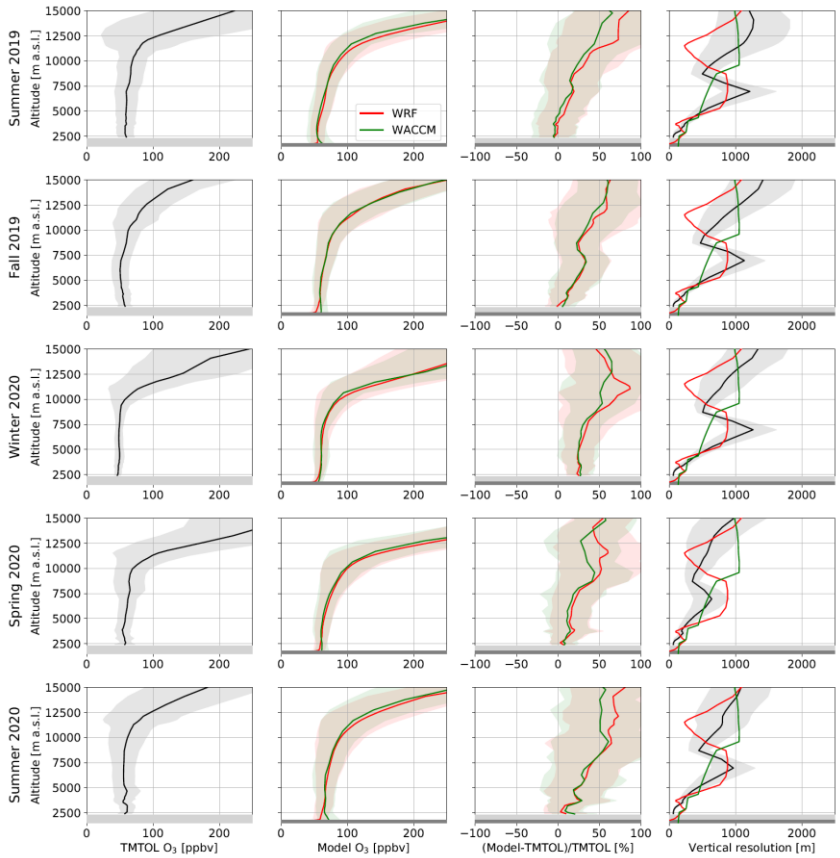

Figure 8. *Relative difference (third column) between TMTOL (first column), WRF-Chem (red) and WACCM (green) ozone profiles (second column) for the period between summer 2019 and summer 2020 (rows). TMTOL retrieval vertical resolution as well as the vertical grid of the models are also shown for each season*

(fourth column). Actual ground level and WRF-Chem surface level are shown as grey and dark grey shaded areas respectively. 1-sigma variability on the ozone profiles and vertical resolution of TMTOL is indicated by the shaded areas.

Additionally, we also performed a comparison of WACCM with the ozonesondes launched at Trinidad Head, CA and Boulder, CO. The preliminary results indicate a similar bias (see below), suggesting that this bias is not particular to TMF, but a more general model feature:

The following was added to the section:

"In order to investigate if this ozone excess is a particular feature of WACCM over TMF, we performed a comparison of the WACCM ozone forecasts and the ECC ozonesondes launched regularly at Trinidad Head, California (about 1000 km north-west from TMF) and Boulder, Colorado (about 1200 km north-east from TMF) for May 2019 to August 2020. The results (Fig. 9) indicate a similar altitude-increasing bias, suggesting a synoptic scale deviation of the forecast for the period under study as a possible reason."

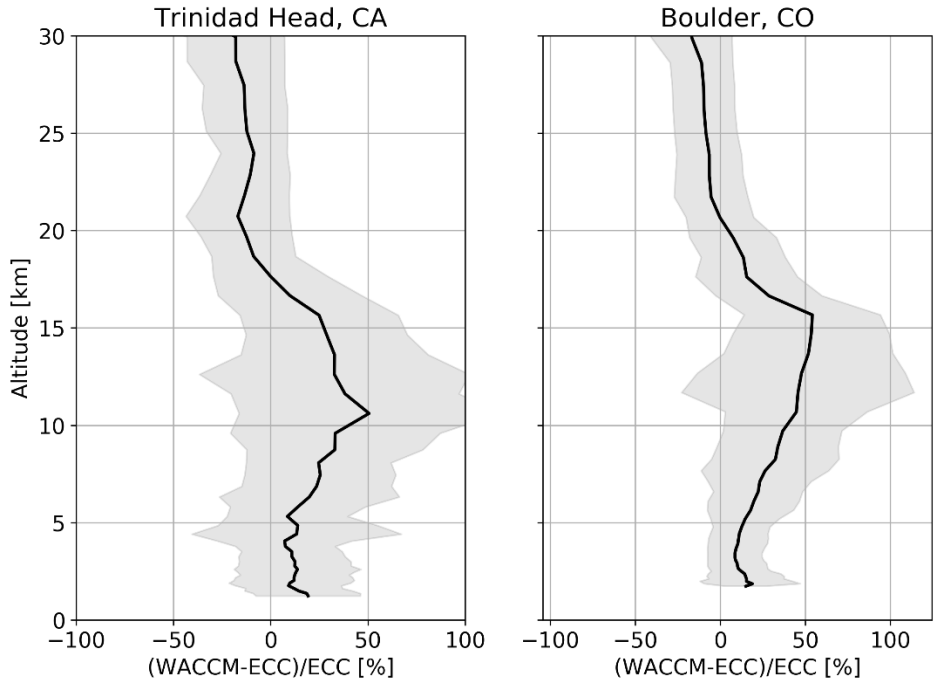

Figure 9. *Relative mean difference between WACCM and ECC ozonesondes during the period comprehended between May 2019 and August 2020 over Boulder, Colorado and Trinidad Head, California. The 1-sigma standard deviation of the difference is indicated by the shaded area.*

Section 4.1. It is indeed an interesting case study to demonstrate the role of stratospheric intrusion for increasing surface ozone measurements at a mountain top station. However it is not a new result which has been reported in several publications. So a discussion is missing either to compare this new case study with previous ones (Bonasoni 2000, Trickl 2019, Knowland 2017) or to explain why the model did not forecast a surface ozone enhancement (line 285 and 300).

The following discussion was added together with an additional figure (note that the figure numbers changed as the case study 1 and case study 2 were switch as suggested by reviewer #1).

"This difference is better depicted in Fig. 13, where ozone, relative humidity and potential temperature as forecasted by WRF-Chem are presented for three different times. The first profile corresponds to the pollution transport event during the late afternoon (A, 0 UTC), with a 500 m deep PBL characterized by an ozone concentration of over 70 ppbv, a relative humidity of almost 30% and a moderately strong temperature inversion at its top. Just above the PBL, and characterized by a relative humidity of 10%, we can see the SI influence forecasted by WACCM and shown in Fig. 12a. As the PBL collapses and the SI approaches the surface, a strong temperature inversion develops near the ground, which inhibits mixing of ozone from the SI and limits its impact in the surface."

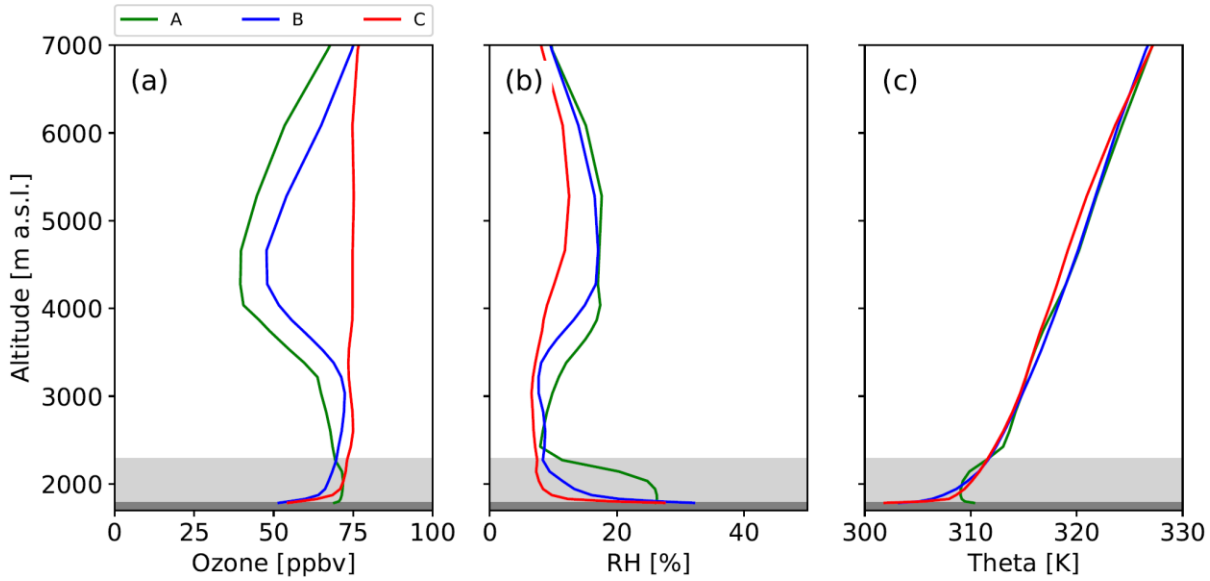

Figure 14. *WRF-Chem ozone, relative humidity and potential temperature over TMF at times A (green, 0 UTC), B (blue, 8 UTC) and C (red, 12 UTC) indicated by red arrows in Fig. 13a top. The actual TMF elevation (light grey shaded) is shown together with the model elevation (grey shaded).*

Line 308 Can the authors use their detailed spatio-temporal analysis of the measured and forecasted ozone field in Figures 9 and 10 in order to discuss the differences in the time series at TMO ? Can a model shift along BB' explain the observations ? Can such a shift explain why the model is too low at the surface or is the model mixing too low in the PBL ?

The cause of the low ozone at the surface is explained in the previous answer.

Figure 10c The dashed line above mountain top is not defined. Is it the PBL top like in figure 9 ? Add a vertical line in Figure 9 at the time corresponding to the horizontal/vertical cross-sections shown in Fig.10. Similar comment for fig. 13 and 11.

Yes, the dashed lines indicate the PBL by the model. The definition was added to the caption. The time of the cross-sections was also added (black arrows on top).

Section 4.2. This case is indeed interesting for the model assessment because the large scale upper tropospheric ozone feature are weaker than case 4.1 and small shift of the modeled ozone field will not easily explain the lidar/model difference.

Section 4.2 (now Section 4.1) is indeed an interesting case, although we consider that the agreement of the upper troposphere feature in this case study as fairly good considering the results presented in Fig. 8. In addition it needs to be considered that this is a forecast product. See also the comparison to the ozonesonde measurements. The main differences are localized in the PBL and lower troposphere, where we have the temporal shift in the ozone maxima as well as a low-level inversion that inhibits mixing and that is challenging to capture by coarser resolution models.

Line 339. Does this kind of model overestimate correspond to the statistical positive bias between model and TMTOL near 3 km which is discussed in section 3.2 ?

This is difficult to say, because most of the profiles of section 3.2 (now section 3.3) corresponds to either noontime (20 UTC) or after sunset (5 UTC +1 day for this case study), which corresponds to either before or after the maxima of pollution transport. For a comparison in the free troposphere, this time difference is not expected to produce a major impact. In the PBL, below 3 km, the impact of this time difference is expected to be larger due to the larger temporal variability.

Line 341 It is worth mentioning that the forecast daily maximum is earlier in the model as previously shown in section 3.1 using the surface observations. It seems to be a permanent feature of the forecast.

Yes, a reference to Sec. 3.1 (now Sec. 3.2) was added to the paragraph.

Line 378 What is the reason for the model performing less for this case study ?

The following was added to the case study discussion:

"This underestimation of the forecasted ozone is likely related to a difference between the forecasted and the actual wind fields. The forecasts show a fairly constant wind direction of 210 degrees (transport from central LA) after 11 June 22:00 UTC, while the measured wind direction at TMF was about 180 degrees (transport from the Fontana/San Bernardino area, south of Crestline). This difference corresponds to two different transport regimes as can be seen in Fig. 4."

Line 344 Is mixing too high in the model close to the ground ?

There is no evidence of a systematic problem regarding the near-ground mixing. As can be seen from the first and second case studies, in one case the model forecasted too much mixing, while in the other it forecasted too little.

Line 413 Although the model/TMTOL differences are lower than 20% within the PBL, it must be stressed that there is a model positive bias which might be related to the large differences observed in the free troposphere between 4 and 7 km.

Some changes were introduced to the conclusion section, including a discussion on the influence of the free troposphere bias in the PBL.

Reviewer #3

General comments

The submitted manuscript submitted by F. Chouza and co-authors concerns the analysis of ozone measurements at the TOLNet/NDACC JPL/Table Mountain (TMO) California station.

The manuscript focuses on the impact of Los Angeles basin pollution transport and stratospheric intrusions on the surface ozone levels observed in the San Gabriel Mountains is investigated based on a combination of surface and lidar measurements as well as WRF-Chem (Weather Research and Forecasting with Chemistry) and WACCM (Whole Atmosphere Community Climate Model) model runs.

This manuscript poses a variety of central thematically relevant questions that could be explored further. The introduction hints at but does not investigate increasing the accuracy of detangling the high-altitude sites (generally use for long term background/clean trends) and their respective local ozone episodes. There is comparisons with model data, but there really isn't a way to extract conclusions that are satisfying in my opinion. The manuscript also begins to describe the ozone NAAQS and ozone exceedance episodes from a regulatory perspective, but does not really go beyond a simple description and table which is not referenced in the case studies later in the manuscript. Many of this has been done previously by the papers referenced within the document (e.g. Cooper, Lin, Langford).

I suggest the authors reorder the manuscript to re-emphasize the new case studies and comment on their regulatory implications in a discussion section. What is clear is the rich and novel data set in the latter half of the manuscript, especially the 2020 episode. This is very appropriate for this journal with a description of new science learned from this case study. This shows clear evidence of the upslope flow/LA basin impact followed directly by a stratospheric intrusion.

Thank you for the comments on the general structure and content of the paper. Based on this comment and the comments from the reviewer #2, we decided to reformulate the introduction to better communicate the main objectives of the paper. In this case, the objectives of the paper are multiple: (1) illustrate the capabilities of the new very-near range receivers to address near-surface pollution transport events. (2) Determine how much of the exceedances relate to SI vs local pollution transport. (3) Evaluate WRF-Chem/WACCM from a general perspective and for the main mechanisms controlling the surface ozone at TMF.

While the case studies are an important part of the paper, they only address part of these points, so we decided to leave them as a second section that complements the first section (more general results).

L23 – Carbon monoxide is not central to the photolysis to generate ozone. CO is certainly a useful tracer. Did you mean OH radical?

'*carbon monoxide*' was removed from the sentence.

L25 – for this site location, is transport notionally from the LA Basin in a regional sense or inter-continental transport on a synoptic scale?

For TMF, as discussed through the paper, the main driver for near-ground ozone variability has been identified as regional transport from the LA basin area. Nevertheless, the impact from the LA basin can extend as far as Las Vegas and probably further away. Unfortunately, the further away the site under study is, the harder is to pinpoint the source to a specific region.

L45 – a "few", is there a way to more quantitatively define this?

The introduction was modified according to your general comments and the comments from the Reviewer #2. There is no more reference to a 'few' stratospheric intrusions.

L75 – is this lidar also part of the NASA TOLNet network? I assume so considering the work in LeBlanc et. Al. 2018.

Yes, the following was added to the end of the sentence:

"and later included to the Tropospheric Ozone Lidar Network (TOLNet)."

Figure 2: What is trying to be conveyed in this z axis? That there is negligible instrument drift? Would a time series be more appropriate? Are the 90ppbv measurements taken during the lidar data shown in subsequent sections? Having a 100m to surface comparison would also be useful to illustrate the gradient on select days.

The idea behind this plot is to show that there is little instrument drift in the bottom part of the retrieval. Since the validation was conducted mainly in clusters of several measurements spaced by a considerable amount of time, a time series would not be the most appropriate way to present them. These measurements do not correspond to any of the case studies shown in Sec. 4. Unfortunately, the validation using the UAV requires physical presence on the measurement site, and all the case studies were conducted remotely due to COVID-associated lockdowns.

Some of this gradient evaluation is part of section 4, where surface measurements are shown together with the 100 m AGL lidar retrieval. Indeed, some interesting gradients were observed (Sec. 4.3 for example).

L118 – If the model does not include stratospheric chemistry, is this really an appropriately rigorous evaluation?

WACCM does include stratospheric and tropospheric chemistry. WRF-Chem boundary conditions are initialized using WACCM forecasts every day. Since the use of WRF-Chem in this study focuses in the lower troposphere, and all stratosphere-related evaluations are based on the WACCM model, we don't see any particular issues with the approach presented on the paper. Actually, we added WACCM to the comparison presented in Sec. 3.3 and the results of WRF-Chem in the upper troposphere are very similar to the results derived for WACCM (which is expected considering that WRF is initialized with WACCM).

Figure 5 – The back-trajectories are difficult to see. Consider alternative approach. Since most of the trajectories are in the same general cardinal direction, why not use a vertical image instead to illustrate the particle dispersion and upslope/mountain chimney effects?

A change in the color of the trajectories was made to improve visibility.

Figure 8 – It is challenging to see a clear result from this figure. Is this an emphasis on showing seasonal changes in ozone or an evaluation of the model? Is the model just not brining enough stratospheric ozone into the troposphere? There is a systematic bias above 7500km. Could this figure be replicated but for a time series of Tropospheric ozone Columns? This product may also be relevant to the upcoming geostationary satellites

Thanks for pointing this out. The figure was mainly focused on the evaluation of WRF-Chem. The idea behind dividing the plot by season was to see if the bias was dependent on the season (and time of the day). We decided to modify this figure to emphasize the validation aspect. This modification includes adding WACCM to the comparison (since it is used to initialize WRF) and remove the day/night profiles (little change was observed between day and night).

Figure 14 – This is the clearest evidence of a LA Basin pollution transport followed by a stratospheric intrusion reaching the western US I have seen. Very appropriate for the journal and the community needs to be aware of these measurements. This should be re-emphasized as the central part of this manuscript.

Thank you for your comments on this. While this is certainly a good example of LA basin pollution/SI influence on near-ground ozone and the model performance, it only addresses part of the objectives listed in the introduction. For this reason, we decided to leave it as part of Sec. 4.

The impact of Los Angeles basin pollution and stratospheric intrusions on the surrounding San Gabriel Mountains as seen by surface measurements, lidar, and numerical models

Fernando Chouza[1], Thierry Leblanc[1], Mark Brewer[1], Patrick Wang[1], Sabino Piazzolla[2], Gabriele Pfister[3], Rajesh Kumar[3], Carl Drews[3], Simone Tilmes[3], Louisa Emmons[3], and Matthew Johnson[4]

[1]Jet Propulsion Laboratory, California Institute of Technology, Wrightwood, CA, USA
[2]Jet Propulsion Laboratory, California Institute of Technology, 4800 Oak Grove Drive, Pasadena, CA, USA
[3]National Center for Atmospheric Research (NCAR), Boulder, CO, USA
[4]NASA Ames Research Center, Moffett Field, CA, USA

Correspondence: Fernando Chouza (keil@jpl.nasa.gov)

Abstract. In this work, the impact of Los Angeles basin pollution transport and stratospheric intrusions on the surface ozone levels observed in the San Gabriel Mountains is investigated based on a combination of surface and lidar measurements as well as WRF-Chem (Weather Research and Forecasting with Chemistry) and WACCM (Whole Atmosphere Community Climate Model) model runs. The number of days with observed surface ozone levels exceeding the National Ambient Air Quality Standards exhibit a clear seasonal pattern, with a maximum during summer, when models suggest a minimum influence of stratospheric intrusions and the largest impact from Los Angeles basin pollution transport. Additionally, measured and modeled surface ozone and PM10 were analyzed as a function of season, time of the day and wind direction. Measurements and models are in good qualitative agreement, with maximum surface ozone observed for south-west and west winds. For the prevailing summer wind direction, slightly south of the ozone maximum and corresponding to south south-west winds, lower ozone levels were observed. Back-trajectories suggest that this is associated with transport from the central Los Angeles basin, where titration limits the amount of surface ozone. A quantitative comparison of the lidar profiles with WRF-Chem and WACCM models revealed good agreement near the surface, with models showing an increasing positive bias as function of altitude, reaching 75% at 15 km above sea level. Finally, three selected case studies covering the different mechanisms affecting the near-surface ozone concentration over the San Gabriel mountains, namely stratospheric intrusions and pollution transport, are analyzed based on surface and ozone lidar measurements, as well as co-located ceilometer measurements and models.

1 Introduction

A high concentration of near-surface ozone poses a hazard to human health (WHO, 2003), animals, and vegetation (Mauzerall and Wang, 2001). Although consistent efforts regulating the emissions of ozone precursors in the Los Angeles (LA) basin region have led to a considerable reduction in the near-surface ozone levels (Pollack et al., 2013), the LA basin is still marked as a non-attainment area (EPA, 2020). For this reason, there has been an increased interest in understanding and modeling

the different processes driving the near-surface ozone concentration with the aim to generate more effective air quality regulation policies (Lin et al., 2017). Tropospheric ozone is mainly produced through photochemical processes involving ~~carbon monoxide and~~ volatile organic compounds in the presence of nitrogen oxides and sunlight (Monks et al., 2015). Additionally, stratospheric intrusions and elevated anthropogenic ozone plumes subject to long-range transport can also increase the tropo-
25 sphere ozone concentration and can, in some specific conditions, affect the near-surface air quality (e.g. Lin et al., 2012b; Knowland et al., 2017; Langford et al., 2018).

The Los Angeles basin shows one of the highest near-surface ozone concentration records in the United States. This is a consequence of several combining factors, including high precursor emissions associated with transportation and industry, high temperatures, and abundant sunlight, as well as meteorological conditions and surrounding mountains that limit the venting of
30 the accumulated smog (Lu and Turco, 1996; Langford et al., 2010).

While somewhat limited by topography and meteorological conditions, long-range transport of LA basin pollution has been identified as a source of high ozone events around the Mojave desert and other locations further away (Langford et al., 2010; VanCuren, 2015). Among the processes driving the transport of LA basin pollution, we can find low-level transport through several passes found between the mountains that surround the LA basin as well as transport over these mountains and injection
35 in the free troposphere caused by the up-slope flow mechanism, also refereed as the mountain chimney effect (Lu and Turco, 1996; Langford et al., 2010; De Wekker and Kossmann, 2015). While models and short-term measurements have been typically used to study these transport processes, no consistent long-term measurements have been conducted to quantify the frequency of these processes and investigate to which extent limited resolution models used for air quality forecasting reproduce them.

Additionally, many mountain-top monitoring stations have been typically assumed to sample free troposphere air and have
40 been used as part of a general effort to investigate long-term trends in background trace gas mixing ratios. While this assumption might be true in some stations or during particular periods, an assessment of the impact of local anthropogenic pollution sources is crucial to determine how well and during which periods this assumption of free troposphere sampling can be considered accurate (Lee et al., 2015; Tsamalis et al., 2014).

In this work, surface and lidar measurements conducted at the Jet Propulsion Laboratory Table Mountain Facility (JPL
45 TMF) in the San Gabriel Mountains (Southern California) ~~for the last eight years and lidar measurements conducted between May 2019 and September 2020 are used~~ are used to address three main objectives. Firstly, to demonstrate the new near-range measurement capabilities of the Table Mountain tropospheric ozone lidar and their value for pollution transport and deep stratospheric intrusion studies. Secondly, to investigate the ~~impact of LA basin pollution on the near-surface measurements carried at this mountain-top site. During the period under study, a few stratospheric intrusion events were recorded. Their~~
50 ~~influence on near-surface ozone is also briefly presented and discussed. Supporting~~ relative impact of regional pollution transport and stratospheric intrusions on the exceedances of the National Ambient Air Quality Standards at TMF, and to determine the representativeness of surface measurements as a proxy for the free troposphere. Finally, to use these surface and vertical profiles to evaluate the performance in complex terrain of the Weather Research and Forecasting model coupled with Chemistry (WRF-Chem) and Whole Atmosphere Community Climate Model (WACCM) forecasts produced daily by the
55 Atmospheric Chemistry Observations and Modeling (ACOM) laboratory at the National Center for Atmospheric Research At-

mospheric (NCAR)~~are also presented and evaluated to investigate how well current regional and global models can reproduce these observations considering the complex nature of the surrounding terrain~~.

The paper is organized as follows. Section 2 provides a general overview of the main characteristics of the LA basin region and the datasets used in this paper, including a description of the ozone lidar and ceilometer, surface instruments deployed at JPL TMF, and the main setup characteristics of the WRF-Chem and WACCM models provided by NCAR ACOM. Section 3 presents an analysis of the relative impacts of pollution transport and stratospheric intrusions to the observed ozone threshold exceedances at TMF, as well as an evaluation of the WRF-Chem forecast ~~over JPL TMF~~ based on ground and vertical profile measurements conducted between May 2019 and September 2020 ~~at TMF~~ (the period during which the model data is available). In section 4, three case studies depicting the main mechanisms driving high surface ozone events at JPL TMF are discussed and compared with the WRF-Chem/WACCM forecast of these events. Finally, a summary of the key findings of this paper is presented in Section 5.

2 Datasets and methods

2.1 Site description and data coverage

JPL Table Mountain Facility (34.38° N; 117.68° W, 2285 m a.s.l.) is located in the San Gabriel mountains (Fig. 1), north of the LA basin and 6 km ~~north-west from~~ northwest of Wrightwood, the closest town. The site ~~host~~ hosts numerous instruments for air composition monitoring, including lidars and surface instruments (Table 1). Despite the high elevation, differential Optical Absorption Spectroscopy (DOAS) measurements by Chen et al. (2011) reported several days with signatures of anthropogenic pollution between late spring and early summer. Although these measurements already provide evidence of the LA basin impact at TMF, measurements based on the differential optical absorption spectroscopy (DOAS) have a limited capability to resolve the vertical extent of these anthropogenic layers. Similar ~~results have been reported~~ conclusions have been reached by Gorham et al. (2010) at Mt. Wilson (34.22° N; 118.06° W, 1742 m a.s.l.), another high elevation site located in the San Gabriel mountains. In that case, ground-based measurements of CO and non-methane hydrocarbons showed repeated signatures of LA basin pollution transport, with a peak occurrence during summer months.

2.2 Table Mountain tropospheric ozone lidar (TMTOL)

TMTOL is an ozone differential absorption lidar (DIAL) that has been under operation at JPL TMF since 1991. Under its original configuration, the system was able to alternate between ozone and aerosol measurements (McDermid et al., 1991). In 1999, the system was redesigned to provide routine measurements of tropospheric ozone in the middle and upper troposphere for the Network for the Detection of Atmospheric Composition Change (NDACC) (McDermid et al., 2002), and later included to the Tropospheric Ozone Lidar Network (TOLNet). This modification included the removal of the aerosol measurement capabilities, a larger telescope, and a receiver based on interference filters in place of the previous spectrometer-based one.

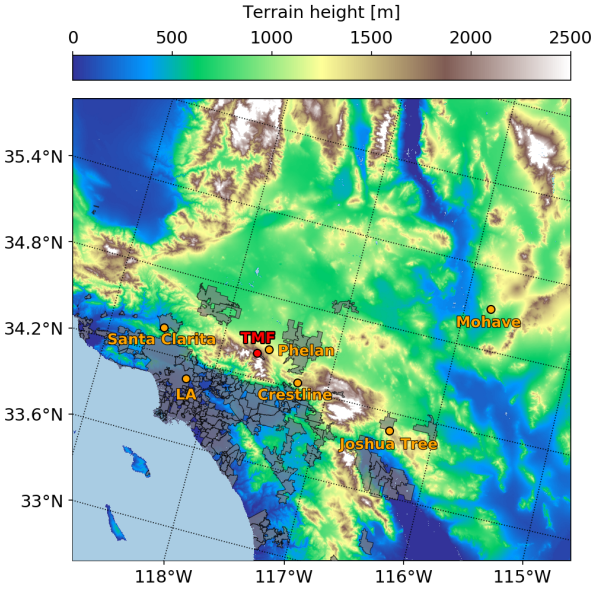

Figure 1. Terrain elevation of the LA basin and Mojave desert area. Urban regions are marked in grey. The location of TMF is marked in red, other surface ozone monitoring stations relevant for this study are marked in orange.

Table 1. Datasets used in this work together with the period under study, temporal resolution and variables analyzed. Except for the two models, all the instruments are located at JPL TMF.

Dataset	Period	Temporal resolution	Variables used in this study
TMTOL	May 2019 - September 2020	~~1 hour~~ 1-hour averaging	O_3 profile (0.1 to $\sim$15 km a.g.l)
CL51	May 2019 - September 2020	$\sim$15 seconds	Attenuated backscatter and boundary layer height
Thermo Fisher 49i	Juanuary 2012 - September 2020	1 minute	Surface O_3
Met One Model 212	May 2019 - September 2020	1 minute	Particle counts (0.3 µm-10 µm)
TMF Met station	May 2019 - September 2020	1 minute	Surface temperature, humidity, pressure and wind
ACOM WRF-Chem	May 2019 - September 2020	1 hour	O_3, anthropogenic CO, boundary layer height and wind
ACOM WACCM	May 2019 - September 2020	6 hours	Stratospheric ozone

In 2018, TMTOL was fully automated and a new channel covering the range between 100 m a.g.l and 1000 m a.g.l was added to the system (Chouza et al., 2019). These two modifications greatly improved the capabilities of the system for air quality and transport studies in the PBL. Long runs of multiple hours or days can be routinely performed without over-stressing the operators, and the retrieved profile extends downwards into the PBL, in contrast to the former setup that allowed only measurements down to 1000 m a.g.l.. In addition to the validation with tethered balloons reported in Chouza et al. (2019), routine validations of this new very-near-range receiver have been conducted with an UAV-borne electrochemical concentration

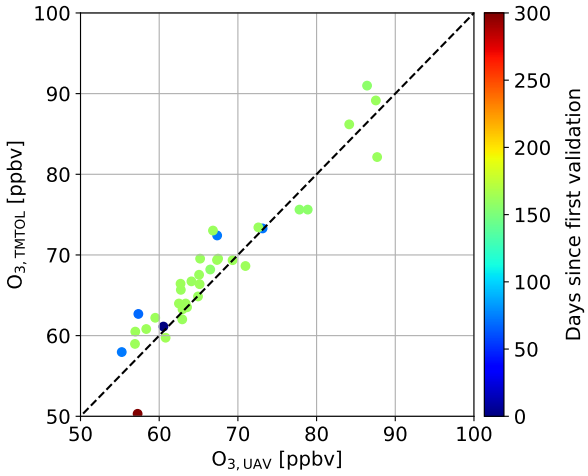

Figure 2. Comparison between the UAV-borne ozonesonde measurements and the corresponding TMTOL retrieval at 100-120 m a.g.l.. The scatter plot color indicates the number of days since the first UAV validation experiment (1 May 2019).

cell (ECC) ozonesonde that provides ozone profiles between the ground and 120 m a.g.l.. The overlap of 20 m between the UAV measurements and TMTOL allows us to verify that the lidar measurement is not biased due to changes in the receiver overlap function. The results of these tests (36 in total) are summarized in Fig. 2. As can be seen, the difference between the first valid TMTOL retrieval and the UAV measurements has been generally under 10%, which is in agreement with previous TMTOL validation studies (Leblanc et al., 2018) and indicate good stability of the very-near-range receiver performance over time.

2.3 Vaisala CL51 ceilometer

Among the atmospheric remote sensing instruments at TMF, a Vaisala CL51 has been operated almost ~~uninterruptedly~~ continuously since 2015. This instrument, located approximately 30 m west ~~from~~ of TMTOL, provides valuable co-located qualitative information regarding the near-surface aerosol layers as well as planetary boundary layer (PBL) height measurements (Wiegner et al., 2014). In this study, the PBL height derivation is obtained from the proprietary Vaisala algorithms included in the original ceilometer software. While the details of this algorithms are not available to the users, a general description can be found in Münkel and Roininen (2010).

2.4 Surface measurements

In addition to TMTOL and the ceilometer, a set of in-situ measurement instruments that provide near-surface measurements of ozone, particulate matter, and meteorological variables are currently deployed at TMF. In the case of surface ozone, measurements are collected by a Thermo Scientific Model 49i Ozone Analyzer that has been operated at TMF since 2013 with

a brief interruption in 2016 due to problems with the instrument. The surface ozone photometer inlet is located at about 2 m a.g.l. on the north side wall of TMTOL building. Particulate matter measurements have been carried out since 2015 by a Met One Model 212, covering particle size from 0.3 µm to 10 µm. This instrument is located about 60 m south ~~from~~ of TMTOL at an altitude of about 2 m a.g.l.. The PM10 values reported in this work have been obtained from the particle counter following Brattich et al. (2020). Since the cut-off diameter of the particle counter is 0.3 µm, an underestimation in the derived PM10 values is expected for fine-mode dominated aerosol events. Finally, meteorological variables including temperature, humidity, and wind speed have been collected with the current setup since 2005 with only a few short interruptions driven by failures in the data acquisition system. The meteorological mast where the instruments are attached is approximately 30 m west ~~from~~ of TMTOL. The wind speed and direction sensor is located at 10 m a.g.l., while the rest of the sensors are at 2 m a.g.l..

2.5 ACOM WRF-Chem forecast

The WRF-Chem air quality predictions are produced daily at NCAR using version 3.9.1 of the WRF-Chem model (Fast et al., 2006; Grell et al., 2005; Powers et al., 2017). The model domain is defined on a lambert conformal project with a horizontal grid spacing of 12 x 12 km^2. The model domain covers the contiguous United States (CONUS) with 390 and 230 grids points in longitudinal and latitudinal directions, respectively. The vertical grid in the model is composed of 43 levels stretching from the surface to 50 hPa. A detailed description (chemical and physical parameterization, emissions, driving meteorological and chemical fields) of the forecasting system configuration can be found at https://www.acom.ucar.edu/firex-aq/tracers.shtml and only details relevant to this study are summarized here.

Tropospheric ozone photochemistry is represented using the Model for Ozone and Related Tracers-4 (MOZART-4) chemical mechanism (Emmons et al., 2010). MOZART-4 contains 83 species that participate in 157 gas-phase reactions and 38 photolysis reactions. The model does not include stratospheric chemistry and lateral boundary conditions control the background as well as upper atmospheric concentrations. In addition, six carbon monoxide (CO) source tracers are included in the model to keep track of CO emitted from anthropogenic and biomass burning emission sources located inside the domain, photochemical production of CO from non-methane volatile organic compounds (NMVOCs) emitted within the domain, and background CO flowing into the domain produced by all non-CONUS sources including non-CONUS fires. CO tracers are subjected to the same physical and chemical losses (reaction with OH and deposition) as the standard CO species is but do not affect any atmospheric processes in the model.

The U.S. EPA National Emissions Inventory (NEI) 2014 is used to represent monthly varying anthropogenic emissions of trace gases and aerosols. No adjustments were made to the emissions due to COVID-19 related restrictions. Fire Inventory from NCAR (FINN) version 1 (Wiedinmyer et al., 2011) provides near-real-time (NRT) biomass burning emissions to the model, which are distributed vertically online within the model using a plume rise parameterization (Freitas et al., 2007). NRT FINN emissions are available with a latency of 1 day and are assumed to persist over the forecast cycle. The meteorological initial and boundary conditions are based on the 00 UTC cycle of the Global Forecast System (GFS) produced daily by the National Oceanic and Atmospheric Administration (NOAA). The chemical boundary conditions are based on the WACCM forecasts produced daily by NCAR (see Sec. 2.6 for WACCM details). The initial conditions for chemical fields are based on previous

day's forecast. Hourly model output is saved for analysis. A two-day model forecast starts at 2 am MT every day and finishes in about 2 hours. Selected model output including concentrations of ozone, PM2.5, key precursor species, meteorological variables, and NRT observations of surface ozone and PM2.5 are displayed at https://www.acom.ucar.edu/firex-aq/forecast.shtml for dissemination to the public.

2.6 ACOM WACCM

The Whole Atmosphere Community Climate Model Version 6 (WACCM6) is one of the atmospheric components of the Community Earth System Model (CESM2) (Gettelman et al., 2019). WACCM6 is a fully coupled global Earth System model that extends from the Earth's surface towards the lower thermosphere ($\sim$ 150 km altitude). The chemistry scheme is the MOZART Troposphere Stratosphere Mesosphere and Low Thermosphere Version 1 (TSMLT1) chemical mechanism (Emmons et al., 2020). The aerosol scheme is the Modal Aerosol Model (MAM4), including a volatility basis set (VBS) description of secondary organic aerosols (Tilmes et al., 2019).

For this study, it uses a horizontal resolution of 0.9° latitude x 1.2° longitude. The specified dynamics version used here adopts the levels of GEOS5 below 50 km and has a total of 88 vertical levels reaching to the model top. The simulation used in this study uses observed sea-surface temperatures and sea-ice conditions for present day that is coupled to the community land model Version 5 (CLM5). The atmospheric winds, temperature, and surface fluxes are nudged below 50 km towards NASA GMAO GEOS5.12 meteorological analysis with a Newtonian relaxation of 50 hours. Daily fire emissions are based on FINNv1. Anthropogenic emissions are from the CAMS Version 3 (Copernicus Atmosphere Monitoring Service) inventory. Biogenic emissions are derived using the Model of Emissions of Gases and Aerosols from Nature version 2.1 incorporated in the CLM (Guenther et al., 2012). A stratospheric ozone tracer is included in this configuration, which is set equal to ozone in the stratosphere and destroyed in the troposphere at the same rate as the model ozone (photochemical destruction and dry deposition).

This model version has been also used to provide a daily 10-day forecast since 2018, using GEOS5 meteorological forecast fields plots and output files that are available at https://www2.acom.ucar.edu/acresp/forecasts-and-near-real-time-nrt-products.

3 ~~WRF-Chem~~ General ozone features and model evaluation

3.1 ~~Surface ozone~~ The impact of pollution transport and ~~PM10~~stratospheric intrusions on high ozone days

While Granados-Muñoz and Leblanc (2016) already provided an overview of the surface ozone characteristics at TMF for the period 2013-2015, additional analysis as well as supporting model information are expected to help to better characterize the impact of the LA basin pollution at TMF. Figure 3a shows a histogram of ozone exceedances based on the surface ozone measurements conducted at TMF from January 2012 to September 2020. Due to a malfunction of the TMF surface ozone analyzer, measurements from 2016 are excluded from this study. While variable from year to year, the number of days with ozone levels exceeding the EPA regulations follow a clear progression over the months, with almost no exceedances during

winter and a large number of exceedances during summer. A remarkably low number of exceedances were observed in 2019, which is likely associated with below-average temperatures (not shown). Since the local production of ozone precursors is very limited in the San Gabriel mountains, the origin of these exceedances is likely related to direct transport from the LA basin region as previously reported in the case study presented in Langford et al. (2010). Together with anthropogenic pollution transport, stratospheric intrusions have also been pointed as the cause of high surface ozone events in the region (Lin et al., 2012a). Since no isotope-based stratospheric tracer measurements (Stohl et al., 2000) are available at TMF, the surface impact of stratospheric intrusions is hard to quantify. Nevertheless, Fig. 3b provides an overview of the stratospheric tracer reported by WACCM at 2700 m a.g.l. since May 2019 over TMF. This figure shows a clear pattern in the number of deep intrusions, with a maximum during winter and early spring, and a minimum during summer and early fall. This seasonality is in agreement with previous studies in the region (Granados-Muñoz and Leblanc, 2016). ~~Together with the box plot, the value~~ On the other hand, Fig. 3c provides an overview of the surface anthropogenic CO contribution forcasted by WRF-Chem, which shows larger median values during summer, when transport of LA basin pollution by the slope mountain effect is expected to be at its maximum. Together with these box plots, the values of the stratospheric ozone contribution reported by WACCM and WRF-Chem anthropogenic CO during exceedance days ~~is~~ are also shown. In most cases, the WACCM stratospheric ozone levels during exceedance days fall within 1.5 times the inter-quartile range (IQR), which suggests that it plays a limited role in most ozone exceedance cases. On the other hand, anthropogenic CO during ozone exceedance days is typically well above the median, which suggests that pollution transport plays a more important role in the ozone exceedances than the stratospheric intrusions. Similarly, relative humidity and temperature are also presented, as intrusions are typically associated with cold fronts and dry air. Temperature and humidity values during ozone exceedance days do not show a major departure from median values. While this analysis does not rule out stratospheric intrusions as the cause of some of the exceedances, their overall impact appears to be limited according to the WACCM ~~model.~~ and WRF-Chem models. Additionally, the concentrations of the anthropogenic CO tracer as forecasted by WRF-Chem appear to be highly variable and generally non-negligible over the whole year, with median values of 12 ppbv during winter and over 25 ppbv during summer, suggesting that surface and near-ground measurements at TMF are strongly influenced by local sources and cannot be generally assumed to be representative of the free troposphere.

3.2 Surface ozone and PM10 as function of time and wind direction

Since LA basin pollution transport seems the most likely cause for the large number of exceedances observed during the March-October period, an analysis of the ozone and PM10 levels as a function of local time and wind direction is presented in Fig. 4 for the period between summer 2019 and summer 2020. Here, summer, fall, winter and spring are defined as June-July-August (JJA), September-October-November (SON), December-January-February (DJF), and March-April-May (MAM) respectively. As supporting information, ozone, PM10, and anthropogenic CO provided by the ACOM WRF-Chem forecast is also included for the same period. The first and fourth rows, which present the number of values observed and ~~forecasted~~ forecast for each time of the day and wind direction, reveal prevailing winds almost exclusively from the south south-west (SSW) during summer and spring with very little temporal variability. During fall and winter, a second prevailing wind direction can be seen coming

from the east north-east (ENE). WRF-Chem shows a very similar pattern, with fewer SSW points during winter and slight changes in the prevailing wind directions.

In the case of the ozone measurements and forecast (second and fifth rows), the largest mean values appear in the summer early night extending in some cases into the next day. In the case of WRF-Chem, the peak in the mean ozone has a similar amplitude but is approximately 3 hours earlier than observed and minimum ozone values during morning time are significantly lower (about 10 ppbv) than the measured ones, which leads to an overestimation of the ozone diurnal cycle amplitude by the model. A comparison of the WRF-Chem surface ozone output with the nearby surface ozone stations of Phelan and Crestline, suggests that this temporal shift in the ozone maximum is a particular feature of the model over TMF, while the underestimation of the ozone levels during morning hours by WRF-Chem is common to all three stations (Fig. A1). The cause of this localized temporal shift is uncertain at this point, but it might be related to the smoothing of the terrain in the model and its impact on the slope mountain effect.

The ozone mean is observed to peak for south-west and west winds, slightly north from the prevailing wind direction. For the prevailing wind direction, the observed ozone levels during summer 2019 and 2020 show surprisingly low values, about 10 ppbv below the values observed for west winds. In the case of the forecast, this feature is well reproduced for summer 2019, while for summer 2020, this feature is less pronounced (note that neither WACCM nor WRF-Chem have emissions adjusted for COVID-related restrictions). To understand the origin of this difference, HYSPLIT/PySplit (Stein et al., 2016; Warner, 2018) back-trajectories based on WRF-Chem meteorological fields for summer 2019 (Fig. 5) and summer 2020 ~~and~~ (Fig. 6) were calculated starting at 2:00 UTC (peak of surface ozone at TMF) for 4 hours, which corresponds to the typical time difference with respect to the ozone maximum in the central LA area (Granados-Muñoz and Leblanc, 2016). These trajectories were separated into two groups, one corresponds to the days where the wind direction was between 250 and 300 degrees (Figs. 5 and 6, first column) and a second group, where the wind direction was between 210 and 240 degrees (Figs. 5 and 6, second column). For both groups, the trajectories were started at 10 m above TMF. Additionally, the mean modeled surface ozone (Figs. 5a,b and 6a,b), NO_2 (Figs. 5c,d and 6c,d) and PM10 (Figs. 5e,f and 6e,f) at the time of the end of the back-trajectories (4 hours before the start, peak ozone in central LA) were calculated for these two groups. The surface ozone pattern, as reported in Lu and Turco (1996), is similar for these two cases, with high ozone in the Santa Clarita/San Fernando Valley area and the eastern LA basin and relatively low surface ozone in the central LA area. ~~This~~ The comparison with the EPA surface ozone monitoring stations (see LA, Santa Clarita, Crestline, and Phelan measurements in Figs. 5a,b and 6a,b) shows a good qualitative agreement with the WRF-Chem output, but with measurements showing generally higher ozone levels at Crestline/Santa Clarita and lower values at the central LA site. The latter can be attributed to enhanced near-surface titration associated with high surface $NO_{~~2~~ x}$ levels (Figs. 5c,d and 6c,d). The trajectories corresponding to the prevailing winds (210-240 degrees) end over this high surface NO_2 region, which likely explains the difference with respect to the ~~west wind~~ 250-300 degrees back-trajectories that mainly end in the San Fernando Valley area. During fall and spring similar patterns are observed, but with an overall lower ozone concentration. As in the summer case, the ~~forecasted~~ forecast nighttime ozone concentration is lower than the observed one. During winter, ~~forecasted~~ forecast and observed ozone exhibits the largest homogeneity among seasons, with very little dependence ~~with~~ on time or wind direction.

During summer 2019, PM10 observations and forecast (third and sixth rows of Fig. 4) exhibited a pattern very similar to the one observed for ozone, with a diurnal cycle peaking in the afternoon for west and north-west winds. For the prevailing SSW winds, a minimum in the PM10 is observed and ~~forecasted. A remarkable difference is nevertheless~~ forecast. A difference is observed for ENE winds, where a second PM10 maximum in the afternoon can be distinguished, likely associated with dust transported from the Mojave desert. During fall and spring, and although there is still a qualitative agreement between measurements and forecast, the ~~forecasted~~ forecast PM10 values are generally larger than the measured ones. The winter PM10 measurements show very little aerosol load, while WRF-Chem shows a pattern similar to spring and summer. In contrast to the observations and forecast presented for summer 2019 and the forecast for summer 2020, summer 2020 PM10 observations shows generally larger concentrations and no minimum associated with south south-west (SSW) winds. The explanation for this discrepancy is unknown, but might be associated with enhanced aerosol load product of extensive wildfires occurred during summer 2020.

Finally, the anthropogenic CO forecast (last row) provides a clear view of the LA transport process, with relatively low seasonal variability (as discussed on Sec. 3.1), a clear maximum in the late afternoon and south to south-west winds.

WRF-Chem was shown to be able to qualitatively reproduce most of the features observed in the spatio-temporal distributions of ozone and PM10 at TMF and the surrounding stations. Some differences were observed regarding the amplitude of the ozone diurnal cycle at TMF and the nearby stations (Figs. 4 and S1). In the particular case of TMF, the forecasted maximum of the ozone diurnal cycle was about 3 hours earlier than the measured maximum. As also shown in Sec. 3.1, the results shown in this subsection indicate that surface ozone concentrations during summer at TMF are strongly influenced by pollution transport from the LA basin region. Transport from central LA, where titration limits the surface ozone concentrations, is characterized by generally lower ozone levels at TMF, while transport from Santa Clarita is generally associated with higher ozone concentrations.

3.3 Vertical ozone profile

While surface measurement instruments like the 49i Ozone Analyzer and the particle counter provide almost continuous datasets (Sec. 3.2), vertical profiles, as obtained by lidars and balloons, are often required to understand the vertical extent, source, and potential for long-range transport of different types of high surface ozone events. In the case of TMF, this is especially true, as the surrounding mountainous terrain adds a layer of complexity to the transport processes and the interpretation of surface measurements.

The previous long-term study presented in Granados-Muñoz and Leblanc (2016) focused ~~in~~ on the free troposphere, as the minimum TMTOL range was mainly limited to 1.3 km a.g.l., which left out of the study most of the PBL. The new very-near range channels, able to reach as low as 100 m a.g.l., have been operated and validated in a routine manner since their installation in mid-2018, allowing almost complete coverage of the PBL. Additionally, during the last two years, longer run periods of multiple days have been regularly conducted by TMTOL in order to capture ~~forecasted~~ forecast SI and LA pollution transport events with the aim to understand the relative contribution of these to the observed exceedances at TMF and investigate to what extent the forecasting tools are able to reproduce them.

While validation of surface ozone and PM forecast is conducted as part of the ACOM WRF-Chem model runs on a routine basis, vertical evaluation is typically restricted to specific locations, as this type of measurement is not nearly as common as the surface ones. In addition to the multi-day runs focused on particular events, TMTOL has continued its regular operations consisting of one hour daily measurements during TROPOMI overpasses (typically around 1 pm local time) and 2-hour measurements 4 to 5 times per week during early nighttime. In this section, all the profiles retrieved from TMTOL since the beginning of the ACOM WRF-Chem forecast runs (May 2019) are used to evaluate the general performance of the model over TMF.

Due to the complex nature of the terrain surrounding TMF, an assessment of the impact of the terrain smoothing associated with the limited spatial resolution of WRF-Chem has to be made. Figure 7 presents an overview of the WRF-Chem terrain elevation in the LA basin area, together with two cross-sections showing the difference between the actual and WRF-Chem terrain elevations. The A-A' cross-section is selected to be parallel to the prevailing winds in the region, while the B-B' is almost perpendicular to A-A' and provides a general view of the passes and mountains that affect the outflow of the LA basin pollution. Both cross-sections were selected to run over TMF.

Thanks to the relative smoothness of the mountains surrounding the LA basin, a fairly good agreement between the actual terrain and the model terrain can be seen along the two cross-sections. The difference at TMF is among the largest ones, with the actual elevation being about 2.3 km and the modeled one about 1.7 km. Since this difference is mainly restricted to the top of the mountain, the effect on the mountain venting process and the associated vertical ascent is expected to be small.

Figure 8 presents an overview of the comparison between TMTOL~~and~~ , WRF-Chem and WACCM for the same period analyzed in Sec. 3.2 (summer 2019 to summer 2020), with each row of the plot corresponding to one season. ~~Additionally, the profiles are separated in nighttime and daytime to investigate the impact of the diurnal cycle in the model performance and the resolution change in the TMTOL retrieval.~~ The first column of Fig. 8 shows the mean and standard deviation (1-sigma) of the TMTOL profiles available for each season ~~and time of the day~~ (a total of 726 profiles)~~, together with the corresponding mean profile~~. The second column shows the mean of the temporally closest WRF-Chem ~~profile~~ and WACCM profiles (excluding profiles corresponding to the model spin-up period) to each TMTOL profile included in the mean shown in the first column, as well as the ~~mean~~ standard deviation of these profiles. The third column presents the mean of the relative difference between each individual TMTOL and corresponding WRF-Chem ~~profile~~and WACCM profiles, as well ~~as the mean~~ a the standard deviation of these differences. In order to perform this comparison, the TMTOL profiles are averaged over each level of the ~~model grid~~models grids. As supporting information, the ~~vertical resolution~~ mean vertical resolution (and corresponding standard deviation) for the TMTOL retrieval (Leblanc et al., 2016), is presented together with the WRF-Chem ~~model~~ and WACCM models vertical resolution in the fourth column. It is important to notice that the TMTOL vertical resolution is mainly controlled by the signal-to-noise ratio and the specified retrieval uncertainty. For a fixed uncertainty, the vertical resolution degrades as the amount of solar background increases. For this reason, the vertical resolution during daytime experiments is generally lower than during nighttime ~~.~~ (see Fig. S2). Additionally, since TMTOL consists of different receivers looking at different altitude ranges, the vertical resolution changes as a function of altitude. This change in receivers can be seen as sharp changes in the vertical resolution at around 3 km and 7-8 km.

Overall, the WRF-Chem forecast shows an excess of ozone across the full range under analysis, independent of season and time of the day (not shown). This excess is limited to about 25% in the PBL, but increases almost monotonically with altitude reaching differences of up to 75% at 15 km. No clear difference in the model bias behavior was observed across the tropopause, typically found between 12 km a.s.l. (winter) and 16 km a.s.l. (summer). With respect to the seasonal trends, a good qualitative agreement between the model and TMTOL is observed, with an ozone increase in the UTLS (upper troposphere lower stratosphere) region, with lower and sharper transitions than during winter.

4 ~~High surface ozone drivers at TMF~~

The observed variability in the free troposphere also shows a clear seasonal dependence, with larger variability during summer and reduced variability during winter. The same seasonal pattern is also visible in the WRF-Chem profiles.

The ~~previous section presented a general overview of the ozone and surface PM10 characteristics at TMF as well as an evaluation of the~~ WACCM forecast shows a very similar behavior to the one described for WRF-Chem, including the altitude-dependent bias. Since the WRF-Chem ~~capabilities to reproduce them. In this section, three case studies are presented to illustrate specific mechanisms by which the surface or near surface ozone concentration at TMF can be affected, and investigate the extent to which~~ chemical boundary conditions are determined by the WACCM forecast (Sec. 2.5), the bias observed in the WRF-Chem ~~is able to reproduce them.~~

3.1 ~~3 July 2020: A deep stratospheric intrusion event~~

~~This case study, based on measurements conducted by TMTOL on 3 July 2020 between 4:50 and 17:50 UTC, illustrates the effect of a deep stratospheric intrusion on the surface ozone concentration at TMF. Since deep stratospheric intrusions typically occur during spring and not necessarily significantly affect the surface ozone concentration, the case study presented in this section represents a rarity in both ways. Additionally, and although WRF-Chem and WACCM forecasted enhanced ozone in the lower free troposphere associated with a SI, WRF-Chem did not forecast an effect on the surface ozone as it finally occurred, which illustrates the challenges associated with modeling the entrainment into the nocturnal surface layer and in complex terrain.~~

~~Figure 13a presents an overview of the forecasted WRF-Chem ozone, anthropogenic CO (grey-shaded contours), PBL height (dashed black), and WACCM stratospheric ozone contribution (hatched contours) for the period comprehended between 2 July 2020 12:00 UTC and 4 July 2020 0:00 UTC. The forecast, which motivated an extended TMTOL run, starts with moderate ozone enhancement in the PBL during 2 July with an associated increase of anthropogenic CO, suggesting transport from the LA basin area. After the collapse of the PBL, a persistent layer of high ozone (about 70 ppbv) is visible between the ground and 3.5~~ runs is likely a result of the bias in the WACCM forecast. In order to investigate if this ozone excess is a particular feature of WACCM over TMF, we performed a comparison of the WACCM ozone forecasts and the ECC ozonesondes launched regularly at Trinidad Head, California (about 1000 km ~~a. s.l., with a small drop around 3 July 6:00 UTC. Until that point, the forecast can be seen as a typical case of LA basin pollution transport, with ozone being injected into the free troposphere after the~~

collapse of the PBL. Nevertheless, after 6:00 UTC, a second increase of the ozone in the lower troposphere is visible, which later extends into an ozone-rich stratospheric air tongue with ozone levels exceeding 70 ppbv. The stratospheric origin of this enhancement is supported by the co-located low relative humidity from WRF-Chem, as well as the stratospheric ozone tracer from WACCM , which shows a contribution of over 30 ppbv on 3 July between 4:00 and 13:00 UTC at about 2.5 north-west from TMF) and Boulder, Colorado (about 1200 km a.s.l.. After 13:00 UTC, and as the PBL starts to grow, the influence of the SI starts to decrease and a new transport wave of LA basin pollution takes over as the main ozone driver in the PBL.

While the models presented in Fig. 13a are in qualitative agreement with the TMTOL measurements north-east of TMF) for May 2019 to August 2020. The results (Fig. 13b) , measurements show a shallower layer with a much stronger enhancement in the ozone levels below 3 a.s.l. and a less defined stratospheric air tongue than the simulation. During the whole measurement period , the observed layer was characterized by ozone levels of over 100 ppbv (as opposed to the 70 ppbv forecasted by WRF-Chem) and low aerosol load levels (Fig. 13c). Another significant difference is related to the surface influence of the SI. Figure 13d presents a time series of forecasted and measured surface and 100 a.g.l. ozone mixing ratio, 9) indicate a similar altitude-increasing bias, suggesting a synoptic scale deviation of the forecast for the period under study as a possible reason.

4 High surface ozone drivers at TMF

The previous section presented a general overview of the ozone and surface PM10 characteristics at TMF as well as the measured relative humidity at TMF. While the an evaluation of the WRF-Chem simulation forecasted an almost constant 50 ppbv surface ozone level, compatible with nighttime background conditions, the 49i Ozone Analyzer shows increasing ozone values after sunset, reaching 90 ppbv between 9:00 and 11:00 UTC. While looking at the 100 a.g.l., no significant difference was observed between the first valid TMTOL data point (100 a.g.l.) and the surface, while the capabilities to reproduce them. In this section, three case studies are presented to illustrate specific mechanisms by which the surface or near surface ozone concentration at TMF can be affected, and investigate the extent to which WRF-Chem model showed a gradient of about 15 ppbv between surface and 100 a. g.l.. is able to reproduce them.

Overview of the model outputs and measurements over TMF between 2 July 12:00 and 4 July UTC. (a) WRF-Chem ozone mixing ratio over TMF (color scale), WRF-Chem anthropogenic CO (grey shaded contours), PBL height (dashed black) and WACCM stratospheric tracer (hatched contours). (b) TMTOL measurements (color scale) and PBL height (black points). The ozonesonde profile is shown overlaid at the time of the launch and surrounded by a black box. (c) Ceilometer-derived attenuated backscatter (color scale) and PBL height (black points). (d) WRF-Chem ozone mixing ratio at surface (solid blue) and 100 a.g.l. (dashed blue) together with the 49i Ozone Analyzer surface ozone measurements (solid red), TMTOL ozone mixing ratio retrieval at 100 a.g.l. (dashed red) and surface relative humidity (solid black).

In order to provide a broader context to this case study, the same variables shown in Fig. 13a for 3 July 6:00 UTC are presented in Fig. 15 for a constant altitude of 2.5 a.s.l. around the LA basin area as well as for the two cross-sections defined in Fig. 7.

~~Horizontal and vertical cross-sections of WRF-Chem and WACCM forecast outputs for 3 July 6:00 UTC. (a) Horizontal cross-section at 2.5 a.s.l. (b) Vertical cross-section along A-A' line. (c) Vertical cross-section along B-B' line. Total forecasted WRF-Chem ozone concentration is shown in a color scale (all panels). WRF-Chem anthropogenic CO levels (grey-shaded contours, all panels), WACCM stratospheric ozone (hatched contours, (b) and (c)) and WRF-Chem winds (arrows, (a)) are also shown.~~

~~The constant altitude cross-section (Fig. 15a) shows a well defined high ozone filament south-west of TMF associated with high speed south winds and low humidity (not shown). Slightly north from TMF, a second plume of high ozone and anthropogenic CO (LA basin pollution) can be seen being displaced by this high ozone filament from stratospheric origin. The cross-sections presented in Figs. 15b and 15c provide an additional overview of the stratospheric tongue geometry as well as the stratospheric contribution forecasted by WACCM (hatched contours). The A-A' cross-section shows also very low ozone over the LA basin area, as usually found during nighttime and suggests that little or no impact of this SI was forecasted.~~

4.1 27-29 May 2020: A LA pollution transport event

Between 27 May and 28 May, two TMTOL extended runs were decided based on the WRF-Chem forecast of high surface ozone and anthropogenic CO levels (grey-shaded contours) associated with LA basin pollution transport (Fig. 10a). For the early part of 27 May (the late afternoon of 26 May if local time is considered), low levels of stratospheric influence were ~~forecasted~~ forecast by WACCM (hatched contours), while during the late part of 27 May and beginning of 28 May, a common case of LA basin pollution transport was expected with no stratospheric influence below 6 km a.s.l.. In this latter case, simulated surface ozone levels were compatible with a surface ozone exceedance event, which triggered the second extended TMTOL run. Figure 10b presents an overview of these two measurement sections, as well as the profile captured by an ozonesonde launched on 28 May 1:22 UTC (Fig. 11, solid) and the ceilometer-derived PBL height (Fig. 10c). During the first measurement section conducted between 27 May 1:24 UTC and 7:30 UTC, homogeneous ozone levels of about 70 ppbv were observed in the PBL, while the free troposphere was characterized homogeneous levels of about 40 ppbv. While TMTOL measurements and WRF-Chem are in qualitative agreement, the observed high ozone levels extended later in the day than the ~~forecasted~~ forecast ones, which is compatible with the general behavior presented in Sec. 3.2. The ceilometer backscatter measurements presented in Fig. 10c show a strong correlation with the TMTOL profiles, with high ozone in the PBL associated with high aerosol levels. ~~In contrast to the previous case study, where large differences were observed between the measured and forecasted surface ozone levels, the~~ Finally, the first part of this case study revealed a good agreement between the forecast and the surface measurement in the peak ozone mixing ratio (Fig. 10d).

In the case of the second TMTOL measurement period, conducted between 27 May 16:30 and 28 May 6:30 UTC, the PBL ozone mixing ratio follows a similar spatio-temporal progression as in the previous measurement section, including a similar temporal displacement in the ozone maximum with respect to the model forecast (see Sec. 3.2), similar PBL height, and comparable ozone levels in the PBL and free troposphere. Despite these similarities, there is an interesting feature that makes this case specially interesting for air quality forecasting. While the simulated surface ozone was expected to exceed the

70 ppbv EPA standard at the transition between 27 May and 28 May, and high ozone levels were measured by TMTOL above 300 m a.g.l., almost no surface impact has been measured associated with the LA pollution transport event (Fig. ~~15~~10d).

The origin of this discrepancy was traced back to two well-mixed near-ground layers bounded by very sharp temperature inversions (Fig. 11b) that prevented the ozone-laden air from LA from being down-mixed and affecting thus the surface ozone concentration. The inversions that bounded these two layers were found at 2480 m a.s.l. and 2660 m a.s.l.. The first layer, the closest one to the ground and about 200 m deep, was characterized by an ozone mixing ratio of about 55 ppbv and relative humidity of 20 %, while the second layer, about 150 m deep exhibited an ozone mixing ratio of about 65 ppbv and relative humidity in the order of 27 %. Sitting on top of these two layers, we can see a 1.5 km deep layer characterized by relative high ozone mixing ratio (75 ppbv peak at 3 km a.s.l.) and a higher relative humidity that the other two layers (37 % at 3 km a.s.l.). The ceilometer profiles ~~capture~~ captured during the second TMTOL experiment shown in Fig. ~~15d~~ 10c exhibit a similar structure, with a relatively aerosol-poor layer below 2660 m a.s.l. and an aerosol-laden layer for the rest of the PBL. Finally, the wind profile presented in Fig. 11c revealed high north-westerly winds at low levels, which rapidly slow down and turn to northerly direction above 2660 m a.s.l.. While WRF-Chem forecast (Fig. 11, dashed) was able to forecast most of the previously mentioned features captured by the ozonesonde, including the undercutting of the LA basin pollution layer by an air mass characterized by lower ozone mixing ratio and lower humidity, the terrain smoothing caused this layer to have a limited impact on the surface, which translated into a large difference with regard to the ~~forecasted~~ forecast surface ozone.

~~As in the previous~~ In order to provide a broader context to this case study, Fig. 12 provides a general overview of the WRF-Chem output for the LA basin and surrounding areas at the closes time ~~from~~ to the ozonesonde profile (28 May 1:00 UTC). The 2500 m horizontal cross-section presented in Fig. 12a reveals a fairly large plume of LA pollution, characterized by high ozone and high anthropogenic CO, being transported eastwards. The A-A' cross-section shows an example of the typical mountain venting (or mountain chimney) effect, which has been previously identified as the main mechanism by which LA basin pollution is transported over the San Gabriel mountains and into the free troposphere (Langford et al., 2010). About 2.5 km a.s.l., a slight decrease in the ozone mixing ratio is visible over TMF on both cross-sections, which corresponds to the same undercutting dry and ozone-poor layer previously discussed. The surrounding Phelan and Crestline stations exhibited an opposite behavior to TMF, with the surface ozone greatly exceeding the EPA threshold and measurements showing generally higher ozone than forecast (Fig. A2).

4.2 3 July 2020: A deep stratospheric intrusion event

This case study, based on measurements conducted by TMTOL on 3 July 2020 between 4:50 and 17:50 UTC, illustrates the effect of a deep stratospheric intrusion on the surface ozone concentration at TMF. Since deep stratospheric intrusions typically occur during spring and not necessarily significantly affect the surface ozone concentration, the case study presented in this section represents a rarity in both ways. Additionally, this case study illustrates the challenges of forecasting the impact of SIs on surface ozone concentration. In particular, the difficulties associated with an accurate representation of the entrainment into the nocturnal surface layer in complex terrain.

Figure 13a presents an overview of the forecast WRF-Chem ozone, anthropogenic CO (grey-shaded contours), PBL height (dashed black), and WACCM stratospheric ozone contribution (hatched contours) for the period comprehended between 2 July 2020 12:00 UTC and 4 July 2020 0:00 UTC. The forecast, which motivated an extended TMTOL run, starts with moderate ozone enhancement in the PBL during 2 July with an associated increase of anthropogenic CO, suggesting transport from the LA basin area. After the collapse of the PBL, a persistent layer of high ozone (about 70 ppbv) is visible between the ground and 3.5 km a.s.l., with a small drop around 3 July 6:00 UTC. Until that point, the forecast can be seen as a typical case of LA basin pollution transport, with ozone being injected into the free troposphere after the collapse of the PBL. Nevertheless, after 6:00 UTC, a second increase of the ozone in the lower troposphere is visible, which later extends into an ozone-rich stratospheric air tongue with ozone levels exceeding 70 ppbv. The stratospheric origin of this enhancement is supported by the co-located low relative humidity from WRF-Chem (Fig. 14b), as well as the stratospheric ozone tracer from WACCM, which shows a contribution of over 30 ppbv on 3 July between 4:00 and 13:00 UTC at about 2.5 km a.s.l.. After 13:00 UTC, and as the PBL starts to grow, the influence of the SI starts to decrease and a new transport wave of LA basin pollution takes over as the main ozone driver in the PBL.

While the models presented in Fig. 13a are in qualitative agreement with the TMTOL measurements (Fig. 13b), measurements show a shallower layer with a much stronger enhancement in the ozone levels below 3 km a.s.l. and a less defined stratospheric air tongue than the simulation. During the whole measurement period, the observed layer was characterized by ozone levels of over 100 ppbv (as opposed to the 70 ppbv forecast by WRF-Chem) and low aerosol load levels (Fig. 13c). Another significant difference is related to the surface influence of the SI. Figure 13d presents a time series of forecast and measured surface and 100 m a.g.l. ozone mixing ratio, as well as the measured relative humidity at TMF. While the WRF-Chem simulation forecast an almost constant 50 ppbv surface ozone level, compatible with nighttime background conditions, the 49i Ozone Analyzer shows increasing ozone values after sunset, reaching 90 ppbv between 9:00 and 11:00 UTC. While looking at the 100 m a.g.l., no significant difference was observed between the first valid TMTOL data point (100 m a.g.l.) and the surface, while the WRF-Chem model showed a gradient of about 15 ppbv between surface and 100 m a.g.l.. This difference is better depicted in Fig. 14, where ozone, relative humidity and potential temperature as forecasted by WRF-Chem are presented for three different times. The first profile corresponds to the pollution transport event during the late afternoon (A, 0 UTC), with a 500 m deep PBL characterized by an ozone concentration of over 70 ppbv, a relative humidity of almost 30 % and a moderately strong temperature inversion at its top. Just above the PBL, and characterized by a relative humidity of 10 %, we can see the SI influence forecasted by WACCM and shown in Fig. 13a. As the PBL collapses and the SI approaches the surface (B and C), a strong temperature inversion develops near the ground, which inhibits mixing of ozone from the SI and limits its impact in the surface.

As in the previous case study, the same variables shown in Fig. 13a for 3 July 6:00 UTC are presented in Fig. 15 for a constant altitude of 2.5 km a.s.l. around the LA basin area as well as for the two cross-sections defined in Fig. 7.

The constant altitude cross-section (Fig. 15a) shows a well defined high ozone filament south-west of TMF associated with high speed south winds and low humidity (not shown). Slightly north from TMF, a second plume of high ozone and anthropogenic CO (LA basin pollution) can be seen being displaced by this high ozone filament from stratospheric origin. The

cross-sections presented in Figs. 15b and 15c provide an additional overview of the stratospheric tongue geometry as well as the stratospheric contribution forecast by WACCM (hatched contours). The A-A' cross-section shows also very low ozone over the LA basin area, as usually found during nighttime and suggests that little or no impact of this SI was forecast.

4.3 11-15 June 2020: A combined case

In this case study, an extended TMTOL run conducted between 10 June 15:20 and 15 June 7:10 UTC is analyzed and compared to the WACCM and WRF-Chem forecasts. In contrast to the previous two case studies, this measurement period provides a more comprehensive and complex picture of the multi-day evolution of the different processes affecting the surface ozone levels at TMF.

During the first two days of this case study, the WRF-Chem and WACCM simulations (Fig. 16a) ~~forecasted~~ forecast little stratospheric influence as well as considerable transport of LA basin pollution during 11 June. TMTOL ozone retrievals (Fig. 16b) and the ceilometer-derived PBL height (Fig. 16b, black) show very good qualitative agreement with the WRF-Chem simulations during 11 June, with larger differences observed during 12 June. During 11 June, a deep PBL reaching 4.5 km a.s.l. (11 June 0:00 UTC) can be inferred from both the forecast and the observations (TMTOL and Ceilometer), with enhanced ozone, anthropogenic CO and aerosol load. In the case of the WRF-Chem simulation, the ozone mixing ratio associated with this transport event was in the order of 70 ppbv at 100 m a.g.l. (Fig. 16d), which agreed well with TMTOL observations. Nevertheless, the simulations also show a very strong gradient in the lower 100 m, which resulted in an underestimation of the impact of this LA basin plume at the surface and prevented the forecasting of the exceedance as it finally happened. In the case of the 12 June forecast, the differences with the TMTOL, ceilometer, and surface instruments were larger compared to the previous day. WRF-Chem simulations ~~forecasted~~ forecast only mild ozone transport, while TMTOL and the ceilometer measurements show ozone mixing ratios over 80 ppbv associated with a strong aerosol load. As in the previous day, the surface ozone records show a second exceedance, while the forecast underestimated the surface impact by about 20 ppbv. ~~A~~ This underestimation of the forecasted ozone is likely related to a difference between the forecasted and the actual wind fields. The forecasts show a fairly constant wind direction of 210 degrees (transport from central LA) after 11 June 22:00 UTC, while the measured wind direction at TMF was about 180 degrees (transport from the Fontana/San Bernardino area, south of Crestline). This difference corresponds to two different transport regimes as can be seen in Fig. 4. Another remarkable feature can be seen on 12 June 13:00 UTC (indicated as 'See text' in Fig. 16c), when the irruption of a thin near-ground layer with high aerosol content made the surface ozone measurements climb briefly up to little under 100 ppbv, while keeping the 100 m a.g.l. TMTOL measurements unaffected.

Starting on 12 June 12:00 UTC, an increase in the stratospheric ozone contribution can be observed developing in WACCM and WRF-Chem forecasts above the PBL. This ozone enhancement, also visible in TMTOL profiles, is followed by two descending ozone-rich stratospheric air tongues. TMTOL observations indicate a good qualitative agreement of the model regarding these two deep intrusions, with some differences on their timing, spatial evolution, and ozone mixing ratio. Shortly after the first intrusion is seen appearing at 7 km a.s.l. (13 June 3:00 UTC), and coincident with the collapse of the PBL, a relatively sharp decrease in the surface ozone mixing ratio from 70 ppbv to 50 ppv can be seen in Fig. 16d. This decrease in

the surface ozone concentration, associated with an increase in the relative humidity, resembles the case study presented in ~~(Chouza et al., 2019)~~ Chouza et al. (2019) and suggest low-level transport of marine air as the source of it. By 13 June 13:00 UTC, the stratospheric intrusion reaches the surface over TMF, causing a decrease in the surface relative humidity and an increase in the surface ozone mixing ratio. The WRF-Chem ozone mixing ratio at 100 m a.g.l. shown in Fig. 16d shows a very good agreement with the TMTOL retrieval at that altitude, while the forecast of the surface ozone shows a considerable underestimation likely associated with the growth of the PBL and limited downward entrainment. In a similar way, the second intrusion is preceded by a decrease in the surface ozone and a strong increase of the relative humidity, associated with marine air transport (back-trajectories not shown). As the SI approaches the surface, the relative humidity decreases, and the surface ozone increases. While the near-ground TMTOL measurements (Fig. 16d) show an ozone mixing ratio peak of about 75 ppbv at the time the intrusion is at its minimum altitude over TMF, the surface ozone and the WRF forecast show only very weak signs of it. Finally, as the PBL starts to grow, the intrusion is pushed up generating a strong gradient between the PBL and the SI with no evident signs of ozone enhancement in the PBL due to entrainment neither in the model or the surface measurements.

The ozone monitoring station in central LA (Fig. A3) did not record any obvious increase in surface ozone associated with any of the two SI events. For the second SI event, the ozone concentration actually dropped more abruptly than forecast, likely related to the onset of the cold front and associated reduced photochemical activity. The Crestline surface monitoring station (the closest high-elevation site to TMF) did show an episodic increase in surface ozone concentrations a few hours before the increase observed at TMF. Surface ozone forecast at the surrounding stations followed the general trend of the observations, but failed to reproduce the SI related increases at the TMF and Crestline station; likely as a result of insufficient entrainment into the nocturnal surface layer. These episodes resemble a case study presented in Langford et al. (2012), where another deep SI was determined to be responsible for an ozone threshold exceedance at the Joshua Tree National Park during 28 May 2010, while the rest of the stations in the LA basin showed a decrease in the ozone concentration as a result of decreased photochemical activity associated with the passage of a cold front.

5 Summary, conclusions and outlook

In the first part of this work, surface measurements conducted at TMF were used, in combination with WRF-Chem and WACCM simulations, to provide an overview of the near-surface ozone and PM10 characteristics at TMF. The results revealed a large number of days with ozone levels exceeding the National Ambient Air Quality Standards at TMF during late spring, summer and early fall, with the maximum during June. During this period, the surface influence of stratospheric intrusions is modeled to be at its minimum. This ~~results~~result, in combination with the large concentrations of anthropogenic CO ~~forecasted~~ forecast by WRF-Chem at TMF, suggests that LA basin pollution plays a dominant role in these exceedance events, regardless of season. Backward-trajectories indicate that the surface ozone at TMF is highly sensitive to the wind regime, with the highest ozone typically observed associated with eastward transport from the Santa Clarita/San Fernando Valley urban area.

Making use of the ~~enhanced spatial and temporal TMTOL measurements capabilitiesallowed by the recently installed very-near range channel and system automation~~recently enhanced TMTOL measurement capabilities, 726 vertical profiles of

ozone ~~measurements conducted~~ measured during TROPOMI overpasses (noon) and shortly after sunset were used to conduct an evaluation of the ACOM WRF-Chem air-quality forecast and WACCM over the period comprehended between May 2019 and September 2020. The comparison revealed a fairly good agreement in the PBL, with ~~an altitude-increasing high-ozone positive bias~~ WRF-Chem generally overestimating the ozone concentration by less than 25%. Above the PBL, a high ozone bias was observed, increasing with altitude and reaching about 75% at 15 km a.s.l.. This bias appears to be season and time-independent~~.~~, and might be partially responsible for the bias observed in the PBL during noon and after sunset. Further measurements during late afternoon, when ozone concentration is expected to be mainly driven by pollution transport from the LA basin, would be required in order to further investigate the impact of the upper troposphere bias in the PBL ozone levels. The comparison with WACCM, used to initialize each of the WRF-Chem runs, revealed a very similar altitude-dependent bias over TMF, Trinidad Head and Boulder, suggesting that the bias is carried over to WRF-Chem from the WACCM runs.

Additionally, three case studies showing stratospheric and LA basin driven exceedances were discussed in light of the WRF-Chem and WACCM stratospheric ozone forecast. A good agreement was observed between TMTOL measurements and simulations concerning the different mechanisms driving near-surface ozone, including LA basin transport through mountain slope effect and stratospheric intrusions. For these case studies, the most distinctive differences between the observations and model regarding the surface ozone levels were observed to be related to near surface temperature inversion that inhibit the down-mixing of the ozone. Additional measurements would be required to evaluate the frequency of these discrepancies.

While the results shown in this work point to the mountain chimney effect and associated LA basin transport as the main mechanism controlling the abundance of ozone and other pollutants in the PBL, residual layers, and lowermost troposphere over TMF, additional datasets including surface measurements of CO, NO_2 and stratospheric tracers (like beryllium-7) would provide additional support to this conclusion and allow a quantification of the actual stratospheric contribution to enhanced ozone levels. Additional lidar measurement capabilities, allowing simultaneous lidar measurements in the LA basin area, TMF, and Mojave desert would provide further evidence of regional transport as well as a better understanding of the impact of these elevated plumes on downwind ozone monitoring stations like those deployed in Mojave and Joshua Tree national parks. Furthermore, the deployment of such lidar systems in ~~the Channel Islands,~~ a coastal environment upwind from the ~~LA~~ L.A. basin, and where the ~~impact~~ influence of local sources is limited ~~(Oltmans et al., 2008)~~(e.g. on the Channel Islands), would allow to better characterize and quantify the tropospheric ozone background conditions of air entering the west coast of the continental United States (Oltmans et al., 2008).

Data availability. The TMTOL data sets used in this study is publicly accessible at https://www-air.larc.nasa.gov/missions/TOLNet/data.html. ACOM WRF-Chem forecast output is accessible at https://www.acom.ucar.edu/firex-aq/FIREX-AQ/Evaluation/TOLNet/Wrightwood_CA/. ACOM WACCM dataset can be requested at https://www.acom.ucar.edu/waccm/download.shtml. Ozonesondes from Trinidad Head, CA and Boulder, CO can be downloaded from ftp://aftp.cmdl.noaa.gov/data/ozwv/Ozonesonde/ For auxiliary datasets, please contact the authors.

Author contributions. Fernando Chouza prepared most of the manuscript and the statistical comparison with the rest of the datasets. Thierry Leblanc is the principal investigator of TMTOL and provided support in analysis of the TMTOL data. Gabriele Pfister, Rajesh Kumar and Carl Drews provided the WRF-Chem forecast used in this study. Simone Tilmes and Louisa Emmons provided the WACCM simulations used in this study. Mark Brewer and Patrick Wang provided technical support for the collection of the data included in this work. Sabino Piazzolla provided the ceilometer and PM10 data. Matthew Johnson provided information used to decide when to run TMTOL (case studies) and input on the lidar-model intercomparison. All co-authors provided feedback on the manuscript.

Competing interests. The authors declare that they have no conflict of interest.

Acknowledgements. The research was carried out at the Jet Propulsion Laboratory, California Institute of Technology under a contract with the National Aeronautics and Space Administration (80NM0018D004). The development of the WRF-Chem forecasting system was supported by the NASA grant 80NSSC18K0681. We would like to acknowledge high-performance computing support from Cheyenne (doi:10.5065/D6RX99HX) provided by NCAR's Computational and Information Systems Laboratory, sponsored by the National Science Foundation. We acknowledge the use of the WRF-Chem preprocessor tool anthro_emis provided by the Atmospheric Chemistry Observations and Modeling Laboratory (ACOM) of NCAR. The National Center for Atmospheric Research is sponsored by the National Science Foundation. We acknowledge NOAA ESRL/GML for the ozonesonde data used in this study.

Appendix A: Appendix A

The following figures provide supporting information for the discussions presented in Sec. 3.2, Sec. 4.1, and Sec. 4.3.

References

Brattich, E., Bracci, A., Zappi, A., Morozzi, P., Di Sabatino, S., Porcù, F., Di Nicola, F., and Tositti, L.: How to Get the Best from Low-Cost Particulate Matter Sensors: Guidelines and Practical Recommendations, Sensors, 20, 3073, https://doi.org/10.3390/s20113073, 2020.

Chen, C. M., Cageao, R. P., Lawrence, L., Stutz, J., Salawitch, R. J., Jourdain, L., Li, Q., and Sander, S. P.: Diurnal variation of midlatitudinal NO_3 column abundance over table mountain facility, California, Atmospheric Chemistry and Physics, 11, 963–978, https://doi.org/10.5194/acp-11-963-2011, 2011.

Chouza, F., Leblanc, T., Brewer, M., and Wang, P.: Upgrade and automation of the JPL Table Mountain Facility tropospheric ozone lidar (TMTOL) for near-ground ozone profiling and satellite validation, Atmos. Meas. Tech., 12, 569–583, https://doi.org/10.5194/amt-12-569-2019, 2019.

De Wekker, S. F. J. and Kossmann, M.: Convective Boundary Layer Heights Over Mountainous Terrain—A Review of Concepts, Front. Earth Sci., 3, 77, https://doi.org/10.3389/feart.2015.00077, 2015.

Emmons, L. K., Walters, S., Hess, P. G., Lamarque, J.-F., Pfister, G. G., Fillmore, D., Granier, C., Guenther, A., Kinnison, D., Laepple, T., Orlando, J., Tie, X., Tyndall, G., Wiedinmyer, C., Baughcum, S. L., and Kloster, S.: Description and evaluation of the Model for Ozone and Related chemical Tracers, version 4 (MOZART-4), Geosci. Model Dev., 3, 43–67, https://doi.org/10.5194/gmd-3-43-2010, 2010.

Emmons, L. K., Schwantes, R. H., Orlando, J. J., Tyndall, G., Kinnison, D., Lamarque, J.-F., Marsh, D., Mills, M. J., Tilmes, S., Bardeen, C., Buchholz, R. R., Conley, A., Gettelman, A., Garcia, R., Simpson, I., Blake, D. R., Meinardi, S., and Pétron, G.: The Chemistry Mechanism in the Community Earth System Model Version 2 (CESM2), J. Adv. Model. Earth Syst., 12, e2019MS001 882, https://doi.org/10.1029/2019MS001882, 2020.

EPA: Nonattainment Areas for Criteria Pollutants (Green Book), https://www.epa.gov/green-book, 2020.

Fast, J. D., Gustafson Jr, W. I., Easter, R. C., Zaveri, R. A., Barnard, J. C., Chapman, E. G., Grell, G. A., and Peckham, S. E.: Evolution of ozone, particulates, and aerosol direct radiative forcing in the vicinity of Houston using a fully coupled meteorology-chemistry-aerosol model, J. Geophys. Res. D: Atmos., 111, https://doi.org/10.1029/2005JD006721, 2006.

Freitas, S. R., Longo, K. M., Chatfield, R., Latham, D., Silva Dias, M. A. F., Andreae, M. O., Prins, E., Santos, J. C., Gielow, R., and Carvalho Jr., J. A.: Including the sub-grid scale plume rise of vegetation fires in low resolution atmospheric transport models, Atmos. Chem. Phys., 7, 3385–3398, https://doi.org/10.5194/acp-7-3385-2007, 2007.

Gettelman, A., Mills, M. J., Kinnison, D. E., Garcia, R. R., Smith, A. K., Marsh, D. R., Tilmes, S., Vitt, F., Bardeen, C. G., McInerny, J., Liu, H.-L., Solomon, S. C., Polvani, L. M., Emmons, L. K., Lamarque, J.-F., Richter, J. H., Glanville, A. S., Bacmeister, J. T., Phillips, A. S., Neale, R. B., Simpson, I. R., DuVivier, A. K., Hodzic, A., and Randel, W. J.: The Whole Atmosphere Community Climate Model Version 6 (WACCM6), J. Geophys. Res. D: Atmos., 124, 12 380–12 403, https://doi.org/10.1029/2019JD030943, 2019.

Gorham, K. A., Blake, N. J., VanCuren, R. A., Fuelberg, H. E., Meinardi, S., and Blake, D. R.: Seasonal and diurnal measurements of carbon monoxide and nonmethane hydrocarbons at Mt. Wilson, California: Indirect evidence of atomic Cl in the Los Angeles basin, Atmos. Environ., 44, 2271–2279, https://doi.org/https://doi.org/10.1016/j.atmosenv.2010.04.019, 2010.

Granados-Muñoz, M. J. and Leblanc, T.: Tropospheric ozone seasonal and long-term variability as seen by lidar and surface measurements at the JPL-Table Mountain Facility, California, Atmos. Chem. Phys., 16, 9299–9319, https://doi.org/10.5194/acp-16-9299-2016, 2016.

Grell, G. A., Peckham, S. E., Schmitz, R., McKeen, S. A., Frost, G., Skamarock, W. C., and Eder, B.: Fully coupled "online" chemistry within the WRF model, Atmos. Environ., 39, 6957–6975, https://doi.org/10.1016/j.atmosenv.2005.04.027, 2005.

Guenther, A. B., Jiang, X., Heald, C. L., Sakulyanontvittaya, T., Duhl, T., Emmons, L. K., and Wang, X.: The Model of Emissions of Gases and Aerosols from Nature version 2.1 (MEGAN2.1): an extended and updated framework for modeling biogenic emissions, Geosci. Model Dev., 5, 1471–1492, https://doi.org/10.5194/gmd-5-1471-2012, 2012.

Knowland, K. E., Ott, L. E., Duncan, B. N., and Wargan, K.: Stratospheric Intrusion-Influenced Ozone Air Quality Exceedances Investigated in the NASA MERRA-2 Reanalysis, Geophys. Res. Lett., 44, 10,691–10,701, https://doi.org/10.1002/2017GL074532, 2017.

Langford, A., Alvarez, R., Brioude, J., Evan, S., Iraci, L., Kirgis, G., Kuang, S., Leblanc, T., Newchurch, M., Pierce, R., Senff, C., and Yates, E.: Coordinated profiling of stratospheric intrusions and transported pollution by the Tropospheric Ozone Lidar Network (TOLNet) and NASA Alpha Jet experiment (AJAX): Observations and comparison to HYSPLIT, RAQMS, and FLEXPART, Atmos. Environ., 174, 1–14, https://doi.org/10.1016/j.atmosenv.2017.11.031, 2018.

Langford, A. O., Senff, C. J., Alvarez II, R. J., Banta, R. M., and Hardesty, R. M.: Long-range transport of ozone from the Los Angeles Basin: A case study, Geophys. Res. Lett., 37, https://doi.org/10.1029/2010GL042507, 2010.

Langford, A. O., Brioude, J., Cooper, O. R., Senff, C. J., Alvarez II, R. J., Hardesty, R. M., Johnson, B. J., and Oltmans, S. J.: Stratospheric influence on surface ozone in the Los Angeles area during late spring and early summer of 2010, Journal of Geophysical Research: Atmospheres, 117, https://doi.org/https://doi.org/10.1029/2011JD016766, https://agupubs.onlinelibrary.wiley.com/doi/abs/10.1029/2011JD016766, 2012.

Leblanc, T., Sica, R. J., Van Gijsel, J. A., Godin-Beekmann, S., Haefele, A., Trickl, T., Payen, G., and Gabarrot, F.: Proposed standardized definitions for vertical resolution and uncertainty in the NDACC lidar ozone and temperature algorithms–Part 1: Vertical resolution, Atmos. Meas. Tech., 9, 4029–4049, 2016.

Leblanc, T., Brewer, M. A., Wang, P. S., Granados-Muñoz, M. J., Strawbridge, K. B., Travis, M., Firanski, B., Sullivan, J. T., McGee, T. J., Sumnicht, G. K., Twigg, L. W., Berkoff, T. A., Carrion, W., Gronoff, G., Aknan, A., Chen, G., Alvarez, R. J., Langford, A. O., Senff, C. J., Kirgis, G., Johnson, M. S., Kuang, S., and Newchurch, M. J.: Validation of the TOLNet lidars: the Southern California Ozone Observation Project (SCOOP), Atmos. Meas. Tech., 11, 6137–6162, https://doi.org/10.5194/amt-11-6137-2018, 2018.

Lee, T. R., Wekker, S. F. J. D., Pal, S., Andrews, A. E., and Kofler, J.: Meteorological controls on the diurnal variability of carbon monoxide mixing ratio at a mountaintop monitoring site in the Appalachian Mountains, Tellus B: Chem. Phys. Meteorol., 67, 25 659, https://doi.org/10.3402/tellusb.v67.25659, 2015.

Lin, M., Fiore, A. M., Cooper, O. R., Horowitz, L. W., Langford, A. O., Levy II, H., Johnson, B. J., Naik, V., Oltmans, S. J., and Senff, C. J.: Springtime high surface ozone events over the western United States: Quantifying the role of stratospheric intrusions, J. Geophys. Res. D: Atmos., 117, https://doi.org/10.1029/2012JD018151, 2012a.

Lin, M., Fiore, A. M., Horowitz, L. W., Cooper, O. R., Naik, V., Holloway, J., Johnson, B. J., Middlebrook, A. M., Oltmans, S. J., Pollack, I. B., Ryerson, T. B., Warner, J. X., Wiedinmyer, C., Wilson, J., and Wyman, B.: Transport of Asian ozone pollution into surface air over the western United States in spring, J. Geophys. Res. D: Atmos., 117, https://doi.org/10.1029/2011JD016961, 2012b.

Lin, M., Horowitz, L. W., Payton, R., Fiore, A. M., and Tonnesen, G.: US surface ozone trends and extremes from 1980 to 2014: quantifying the roles of rising Asian emissions, domestic controls, wildfires, and climate, Atmos. Chem. Phys., 17, 2943–2970, https://doi.org/10.5194/acp-17-2943-2017, 2017.

Lu, R. and Turco, R. P.: Ozone distributions over the los angeles basin: Three-dimensional simulations with the smog model, Atmos. Environ., 30, 4155–4176, https://doi.org/10.1016/1352-2310(96)00153-7, 1996.

Mauzerall, D. L. and Wang, X.: Protecting agricultural crops from the effects of tropospheric ozone exposure: reconciling science and standard setting in the United States, Europe, and Asia, Annu. Rev. Energy Env., 26, 237–268, 2001.

McDermid, I. S., Haner, D. A., Kleiman, M. M., Walsh, T. D., and White, M. L.: Differential absorption lidar systems for tropospheric and stratospheric ozone measurements, Opt. Eng., 30, https://doi.org/10.1117/12.55768, 1991.

McDermid, I. S., Beyerle, G., Haner, D. A., and Leblanc, T.: Redesign and improved performance of the tropospheric ozone lidar at the Jet Propulsion Laboratory Table Mountain Facility, Appl. Opt., 41, 7550–7555, https://doi.org/10.1364/AO.41.007550, 2002.

Monks, P. S., Archibald, A. T., Colette, A., Cooper, O., Coyle, M., Derwent, R., Fowler, D., Granier, C., Law, K. S., Mills, G. E., Stevenson, D. S., Tarasova, O., Thouret, V., von Schneidemesser, E., Sommariva, R., Wild, O., and Williams, M. L.: Tropospheric ozone and its precursors from the urban to the global scale from air quality to short-lived climate forcer, Atmos. Chem. Phys., 15, 8889–8973, https://doi.org/10.5194/acp-15-8889-2015, 2015.

Münkel, C. and Roininen, R.: Investigation of boundary layer structures with ceilometer using a novel robust algorithm, Tech. rep., American Meteorological Society, 2010.

Oltmans, S. J., Lefohn, A. S., Harris, J. M., and Shadwick, D. S.: Background ozone levels of air entering the west coast of the US and assessment of longer-term changes, Atmos. Environ., 42, 6020–6038, 2008.

Pollack, I. B., Ryerson, T. B., Trainer, M., Neuman, J. A., Roberts, J. M., and Parrish, D. D.: Trends in ozone, its precursors, and related secondary oxidation products in Los Angeles, California: A synthesis of measurements from 1960 to 2010, J. Geophys. Res. D: Atmos., 118, 5893–5911, https://doi.org/10.1002/jgrd.50472, 2013.

Powers, J. G., Klemp, J. B., Skamarock, W. C., Davis, C. A., Dudhia, J., Gill, D. O., Coen, J. L., Gochis, D. J., Ahmadov, R., Peckham, S. E., Grell, G. A., Michalakes, J., Trahan, S., Benjamin, S. G., Alexander, C. R., Dimego, G. J., Wang, W., Schwartz, C. S., Romine, G. S., Liu, Z., Snyder, C., Chen, F., Barlage, M. J., Yu, W., and Duda, M. G.: The Weather Research and Forecasting Model: Overview, System Efforts, and Future Directions, Bull. Am. Meteorol. Soc., 98, 1717–1737, https://doi.org/10.1175/BAMS-D-15-00308.1, 2017.

Stein, A. F., Draxler, R. R., Rolph, G. D., Stunder, B. J. B., Cohen, M. D., and Ngan, F.: NOAA's HYSPLIT Atmospheric Transport and Dispersion Modeling System, Bull. Am. Meteorol. Soc., 96, 2059–2077, https://doi.org/10.1175/BAMS-D-14-00110.1, 2016.

Stohl, A., Spichtinger-Rakowsky, N., Bonasoni, P., Feldmann, H., Memmesheimer, M., Scheel, H., Trickl, T., Hübener, S., Ringer, W., and Mandl, M.: The influence of stratospheric intrusions on alpine ozone concentrations, Atmos. Environ., 34, 1323–1354, https://doi.org/10.1016/S1352-2310(99)00320-9, 2000.

Tilmes, S., Hodzic, A., Emmons, L. K., Mills, M. J., Gettelman, A., Kinnison, D. E., Park, M., Lamarque, J.-F., Vitt, F., Shrivastava, M., Campuzano-Jost, P., Jimenez, J. L., and Liu, X.: Climate Forcing and Trends of Organic Aerosols in the Community Earth System Model (CESM2), J. Adv. Model. Earth Syst., 11, 4323–4351, https://doi.org/10.1029/2019MS001827, 2019.

Tsamalis, C., Ravetta, F., Gheusi, F., Delbarre, H., and Augustin, P.: Mixing of free-tropospheric air with the lowland boundary layer during anabatic transport to a high altitude station, Atmos. Res., 143, 425–437, https://doi.org/10.1016/j.atmosres.2014.03.011, 2014.

VanCuren, R.: Transport aloft drives peak ozone in the Mojave Desert, Atmos. Environ., 109, 331–341, https://doi.org/10.1016/j.atmosenv.2014.09.057, 2015.

Warner, M. S.: Introduction to PySPLIT: a Python toolkit for NOAA ARL's HYSPLIT model, Comput. Sci. Eng., 20, 47–62, https://doi.org/10.1109/MCSE.2017.3301549, 2018.

WHO: Health aspects of air pollution with particulate matter, ozone and nitrogen dioxide: report on a WHO working group, Bonn, Germany 13-15 January 2003, 2003.

Wiedinmyer, C., Akagi, S. K., Yokelson, R. J., Emmons, L. K., Al-Saadi, J. A., Orlando, J. J., and Soja, A. J.: The Fire INventory from NCAR (FINN): a high resolution global model to estimate the emissions from open burning, Geosci. Model Dev., 4, 625–641, https://doi.org/10.5194/gmd-4-625-2011, 2011.

Wiegner, M., Madonna, F., Binietoglou, I., Forkel, R., Gasteiger, J., Geiß, A., Pappalardo, G., Schäfer, K., and Thomas, W.: What is the benefit of ceilometers for aerosol remote sensing? An answer from EARLINET, Atmos. Meas. Tech., 7, 1979–1997, https://doi.org/10.5194/amt-7-1979-2014, 2014.

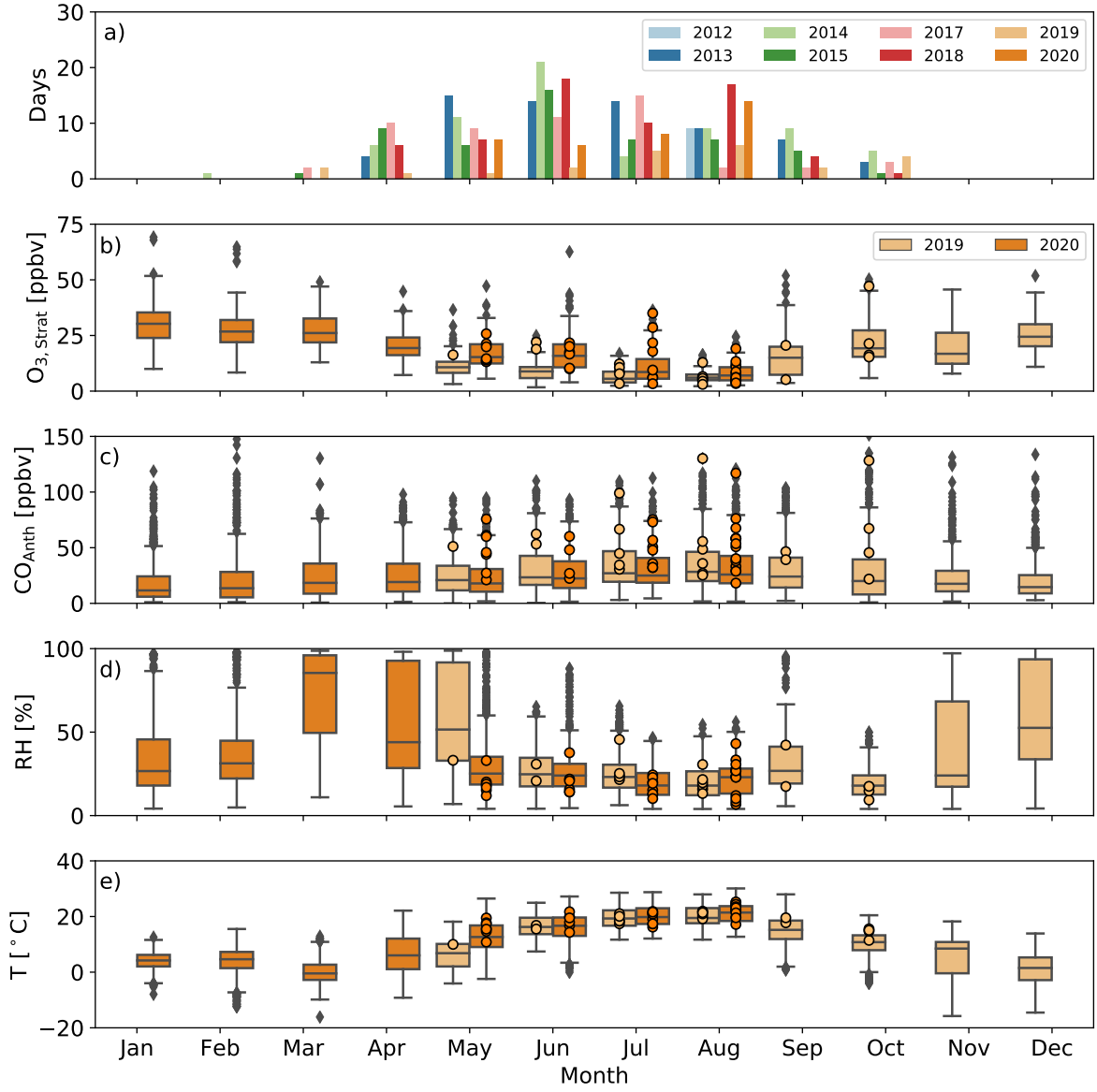

Figure 3. (a) Number of days exceeding the EPA maximum ozone regulations (>70 ppbv 8h MDA) as function of month and year between 2012 and June ~~2020.~~ 2020 derived from the TMF 49i surface ozone monitor. (b) WACCM forecast of the stratospheric ozone at 2700 m a.s.l. as function of month and year between May 2019 and June 2020 presented as a box plot. ~~The WACCM stratospheric ozone values~~ (c) WRF-Chem anthropogenic CO levels for the ~~exceedance days are~~ same period shown ~~as a scatter plot~~in (b). (~~e,~~d,e) ~~Surface~~ Measured surface relative humidity and temperature for the same period presented in (b). ~~Relative~~ WACCM stratospheric ozone, WRF-Chem anthropogenic CO, relative humidity and temperature ~~measurements~~ during the exceedance days are shown ~~as scatter plots~~for comparison (light and dark orange dots). Values exceeding 1.5 times the interquartile range (whiskers) are also shown (black diamonds).

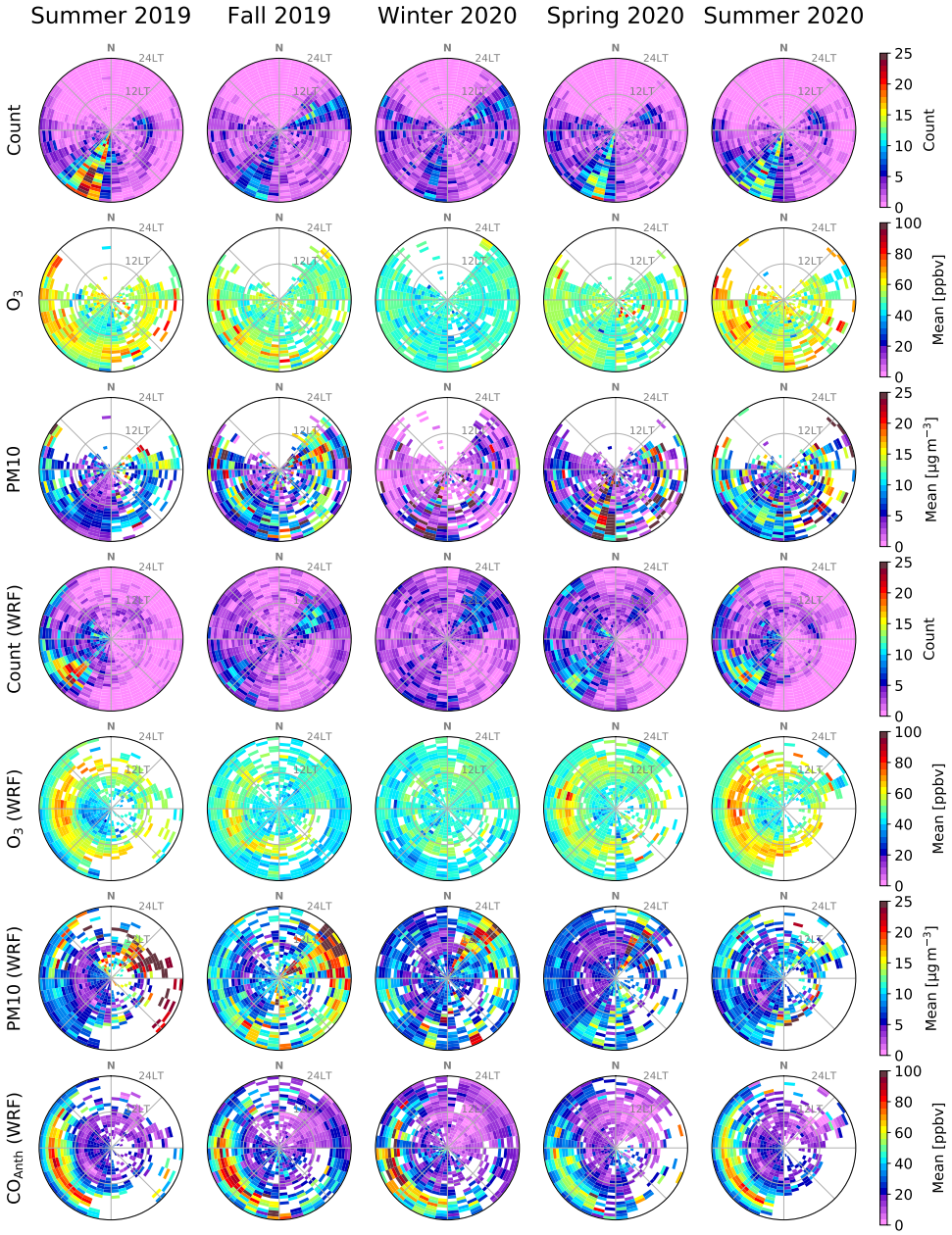

Figure 4. Overview of the number of surface measurements (first row), mean ozone (second row) and mean PM10 (third row) at TMF as function of the time of the day (radial direction, local time), wind direction (angular) and season (columns) for the period comprehended between June 2019 and September 2020. The corresponding values ~~forecasted~~ forecast by WRF-Chem are presented in the fourth, fifth and sixth rows, with the addition of the anthropogenic CO contribution (last row).

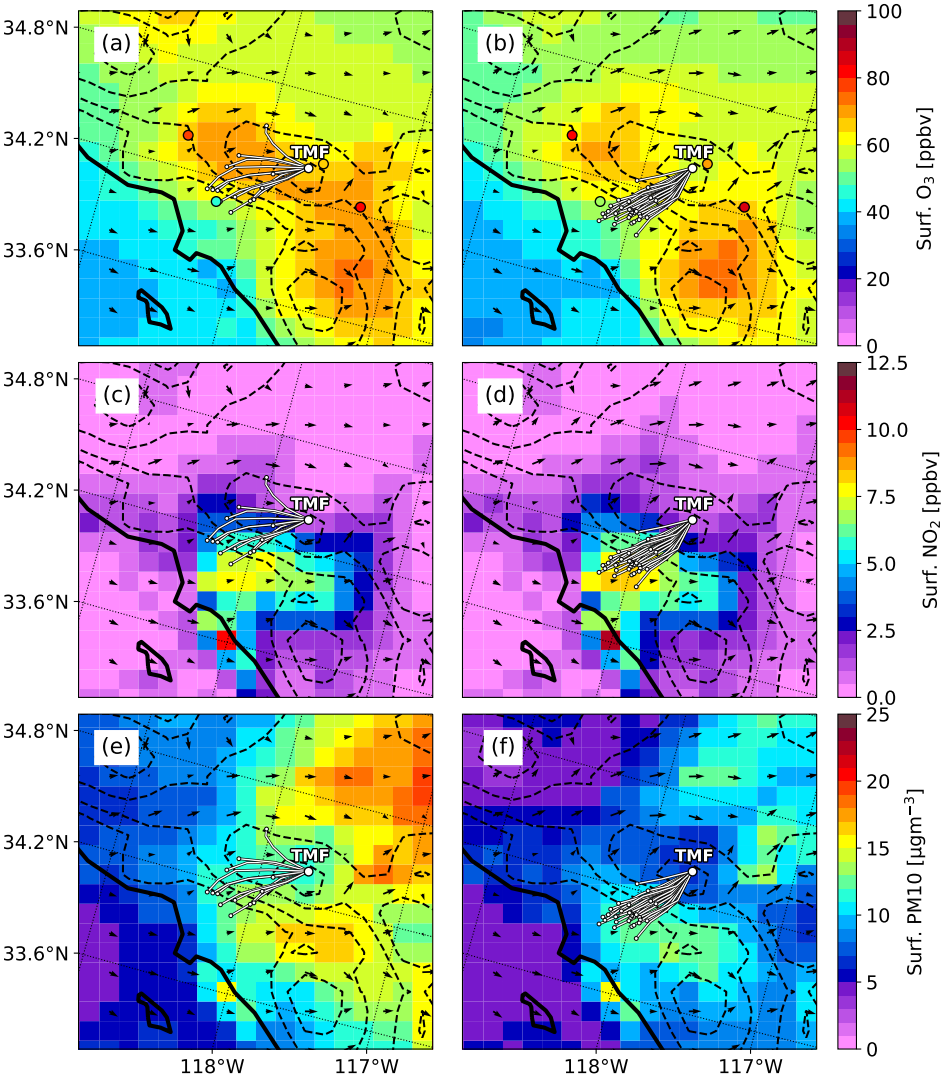

Figure 5. Back-trajectories (~~grey~~white with black borders) started at TMF at 2:00 UTC and ended at 22:00 UTC (-1 day) are shown together with the corresponding mean modeled surface O_3 (a,b), NO_2 (c,d) and PM10 (e,f) at the time of the end of the trajectories for two TMF wind direction groups during summer 2019. (a,c,e) Trajectories started on days where the surface winds over TMF were between 250 and 300 degrees at 2:00 UTC. (b,d,f) Trajectories started on days where surface winds over TMF were between 210 and 240 degrees. 10-m winds are also shown (black arrows). Elevation contours are shown (dashed black) for 250, 500, 1000 and 1500 m a.s.l.. The mean measured surface ozone values are shown as dots (black border) for LA, Santa Clarita, Phelan, and Crestline stations in panels (a,b).

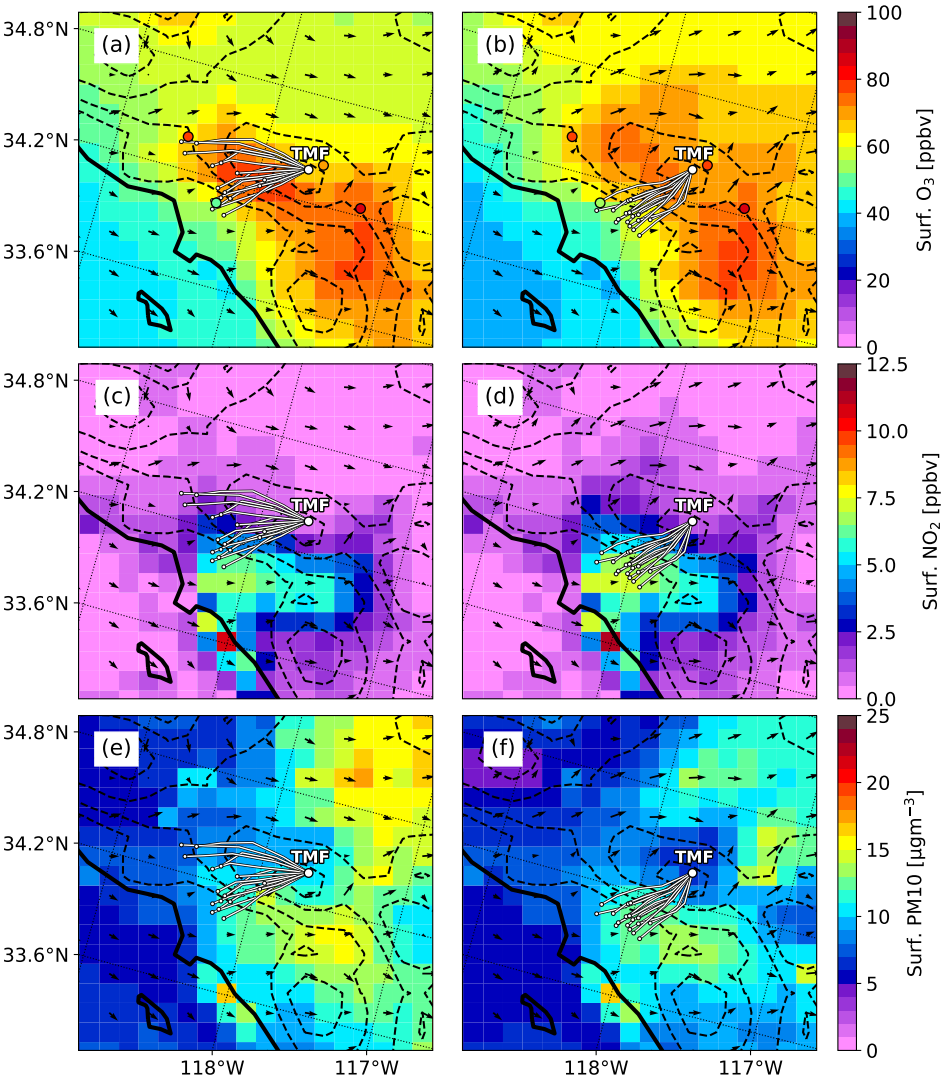

Figure 6. Same as Fig. 5, but for summer 2020.

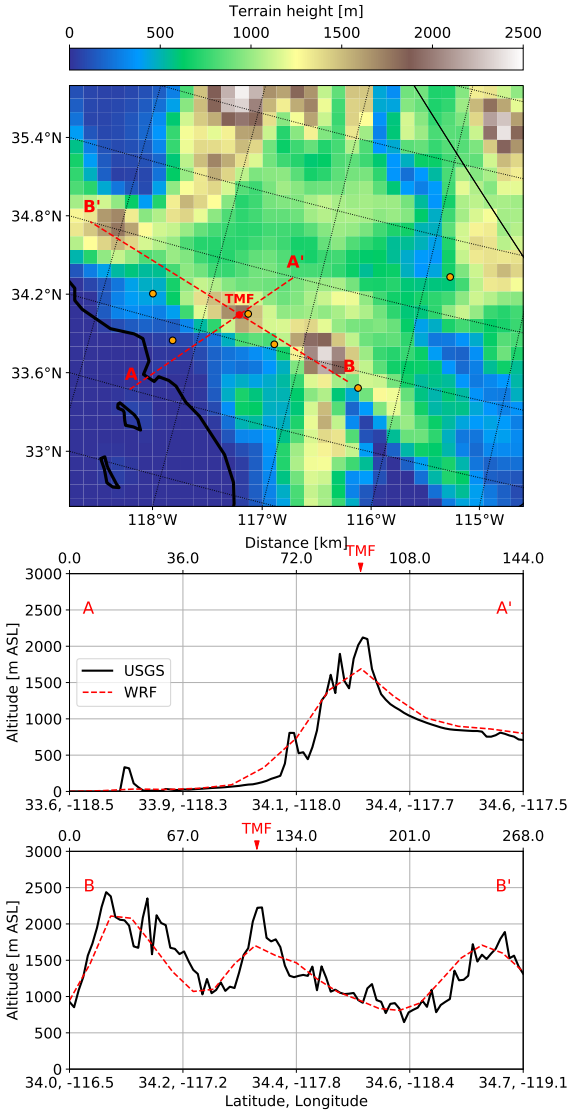

Figure 7. Overview of the terrain elevation used as part of the WRF-Chem simulation for the area under study. The TMF location, as well as the actual (solid, black) and WRF-Chem (dashed red) elevation profiles are shown two selected cross-sections used in this study.

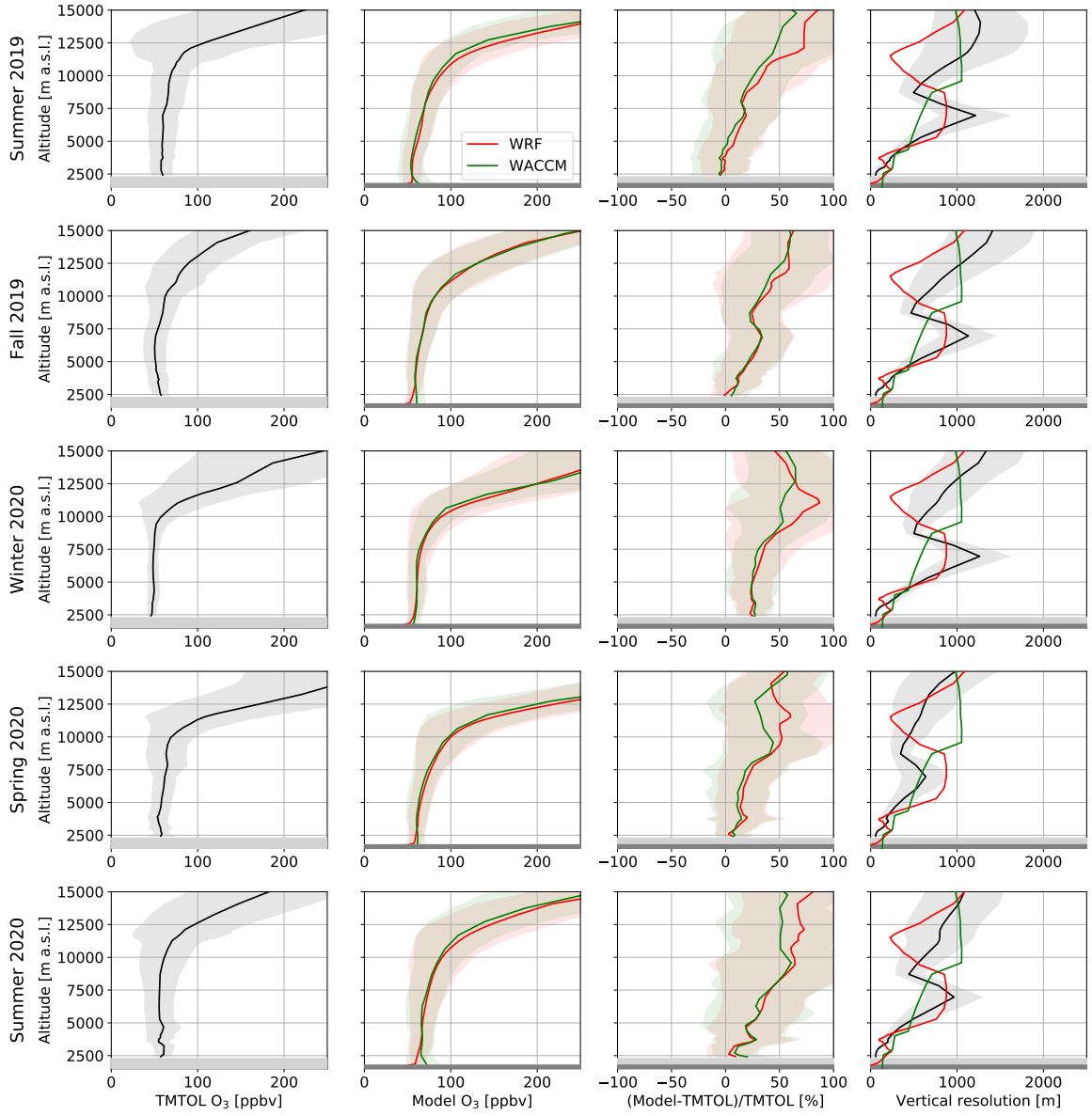

Figure 8. Relative difference (third column) between TMTOL (first column)~~and~~ , WRF-Chem (~~second column~~red) and WACCM (green) ozone profiles (second column) for the period between summer 2019 and summer 2020 (rows). ~~Individual profiles are shown (thin lines) together with the corresponding seasonal mean (thick lines) for daytime (red) and nighttime (blue) profiles.~~ TMTOL retrieval vertical resolution ~~(thin lines)~~ as well as the ~~model~~ vertical grid ~~(dashed black)~~ of the models are also shown for each season ~~and time of the day~~ (fourth column). Actual ground level and WRF-Chem surface level are shown as grey and dark grey shaded areas respectively. 1-sigma variability on the ozone profiles and vertical resolution of TMTOL is indicated by the shaded areas.

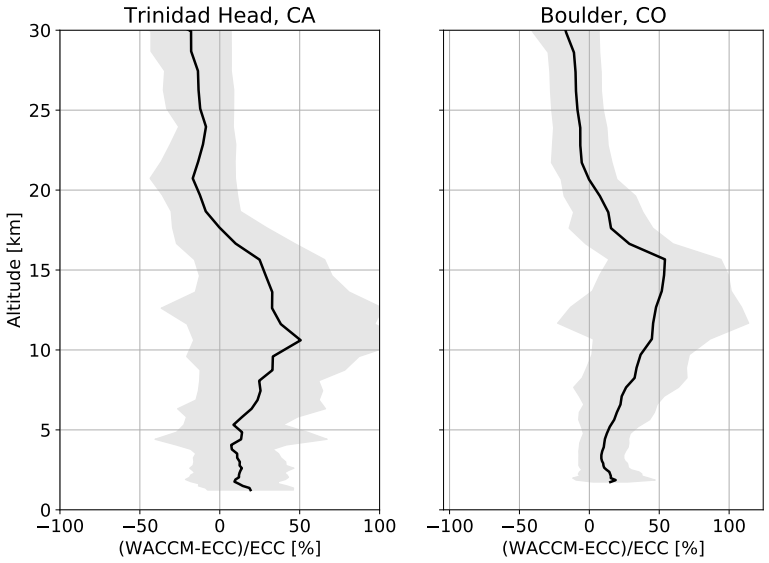

Figure 9. Relative mean difference between WACCM and ECC ozonesondes during the period comprehended between May 2019 and August 2020 over Boulder, Colorado and Trinidad Head, California. The 1-sigma standard deviation of the difference is indicated by the shaded area.

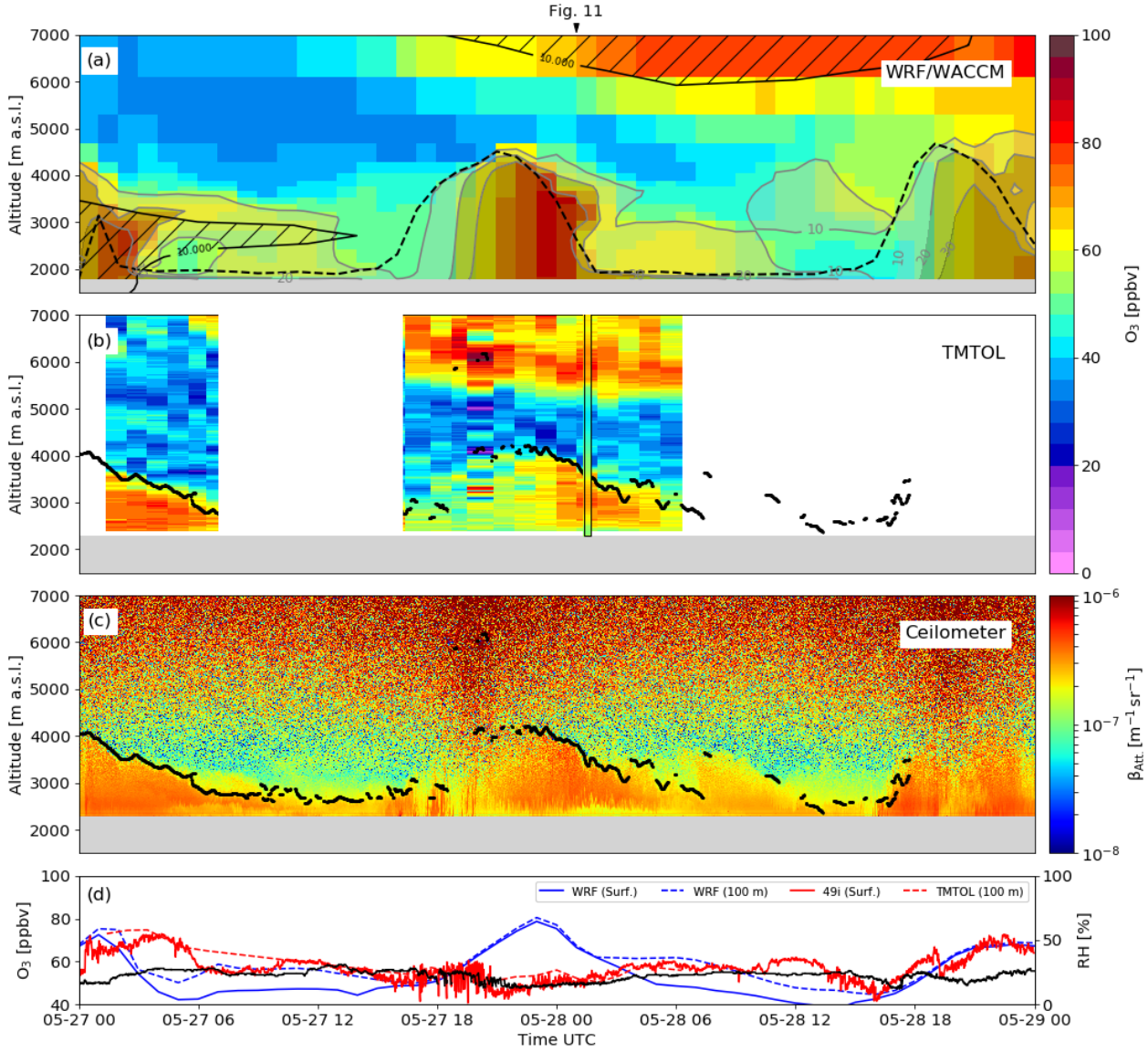

Figure 10. Overview of the model outputs and measurements over TMF between 27 May and 29 May UTC. ~~Panel descriptions are~~ (a) WRF-Chem ozone mixing ratio over TMF (color scale), WRF-Chem anthropogenic CO (grey shaded contours), PBL height (dashed black) and WACCM stratospheric tracer (hatched contours). (b) TMTOL measurements (color scale) and PBL height (black points). (c) Ceilometer-derived attenuated backscatter (color scale) and PBL height (black points). (d) WRF-Chem ozone mixing ratio at surface (solid blue) and 100 m a.g.l. (dashed blue) together with the ~~same as the ones shown for Fig~~49i Ozone Analyzer surface ozone measurements (solid red), TMTOL ozone mixing ratio retrieval at 100 m a.~~13~~g.l. (dashed red) and surface relative humidity (solid black). The ozonesonde profile is shown overlaid at the time of the launch and surrounded by a black box.

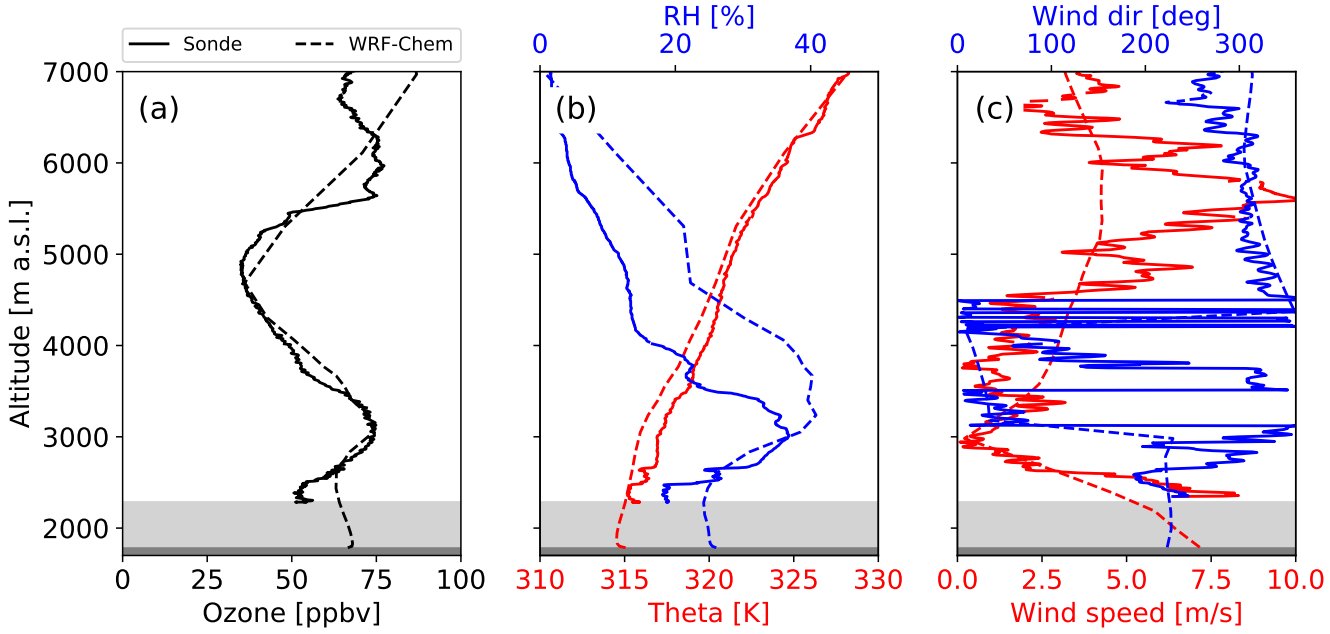

Figure 11. Sonde and corresponding WRF-Chem profiles for the launch conducted on 28 May 1:22 UTC. (a) Sonde ozone profile (solid black) and corresponding WRF-Chem output (dashed black). (b) Sonde-derived potential temperature (solid red) and relative humidity (solid blue) together with the corresponding WRF-Chem profiles (dashed, same colors). (c) Sonde-derived wind speed (solid red) and direction (solid blue) together with the corresponding WRF-Chem profiles (dashed, same colors). The actual TMF elevation (light grey shaded) is shown together with the model elevation (grey shaded).

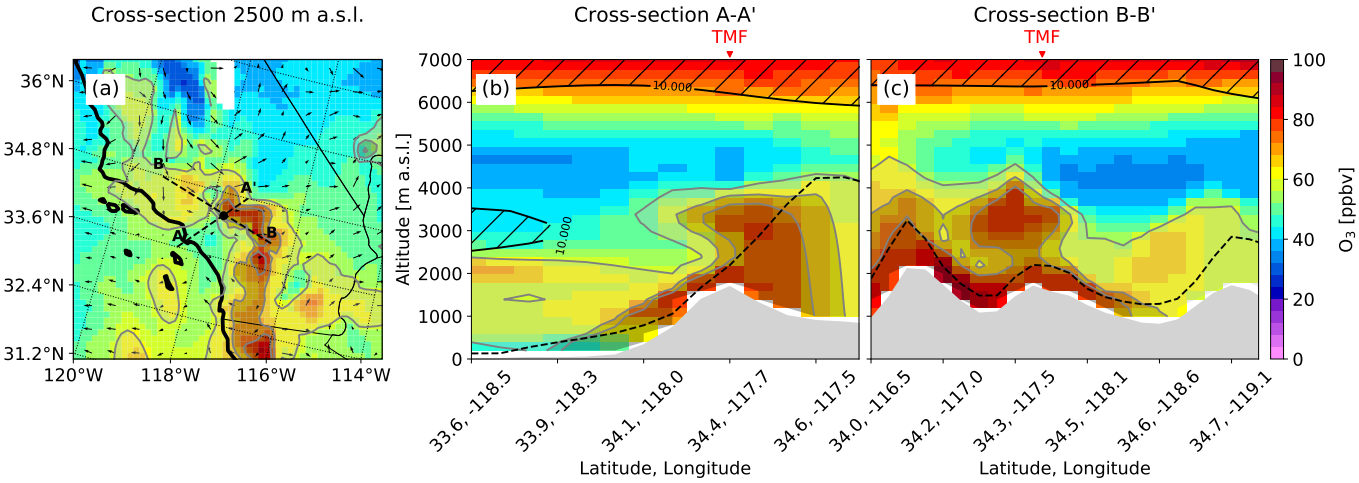

Figure 12. Horizontal and vertical cross-sections of WRF-Chem and WACCM forecast outputs for 28 May 1:00 UTC. ~~Panel descriptions~~ (a) Horizontal cross-section at 2.5 km a.s.l. (b) Vertical cross-section along A-A' line. (c) Vertical cross-section along B-B' line. Total forecast WRF-Chem ozone concentration is shown in a color scale (all panels). WRF-Chem anthropogenic CO levels (grey-shaded contours, all panels), WACCM stratospheric ozone (hatched contours, (b) and (c)), PBL height (dashed black), and WRF-Chem winds (arrows, (a)) are ~~the same as the ones~~ also shown~~for Fig.15.~~

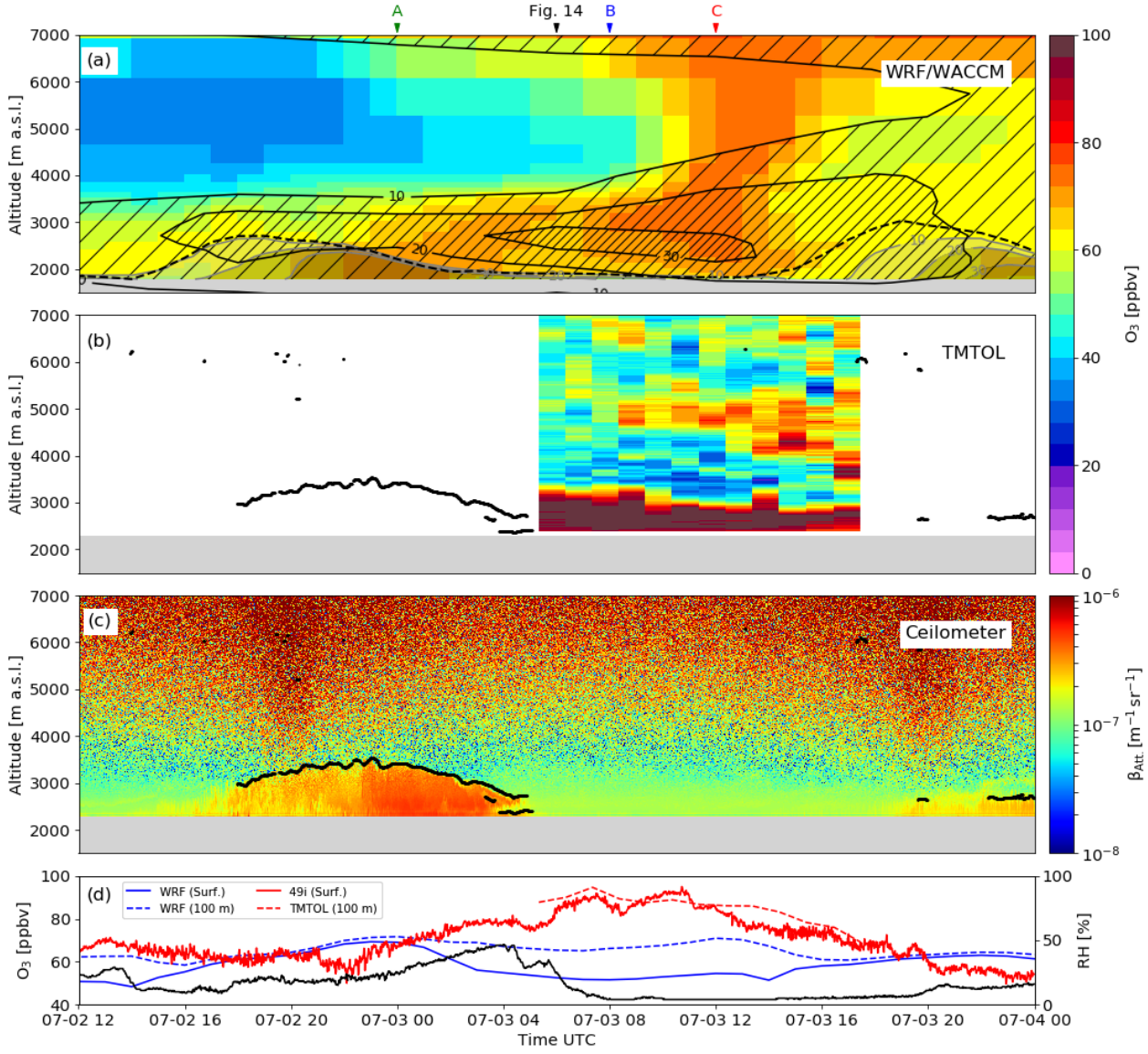

Figure 13. Overview of the model outputs and measurements over TMF between 2 July 12:00 and 4 July UTC. Panel descriptions are the same as the ones shown for Fig. 10. The time of the profiles shown in Fig. 14 are shown as red arrows.

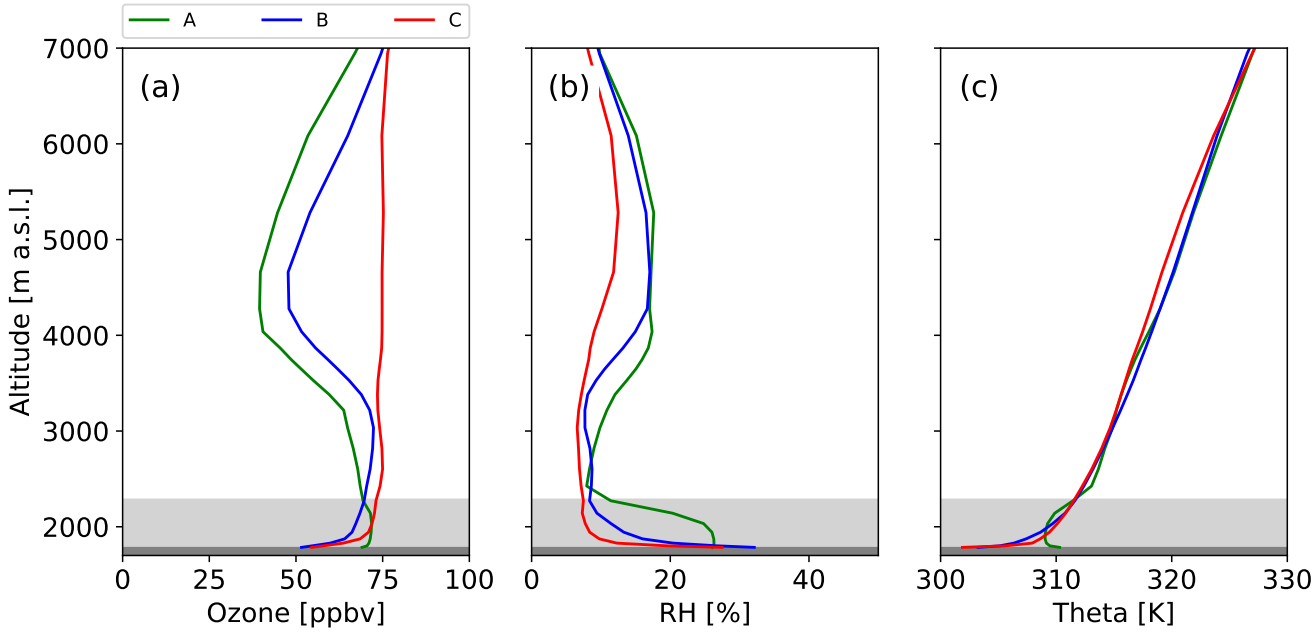

Figure 14. WRF-Chem ozone, relative humidity and potential temperature over TMF at times A (green, 0 UTC), B (blue, 8 UTC) and C (red, 12 UTC) indicated by red arrows in Fig. 13a top. The actual TMF elevation (light grey shaded) is shown together with the model elevation (grey shaded).

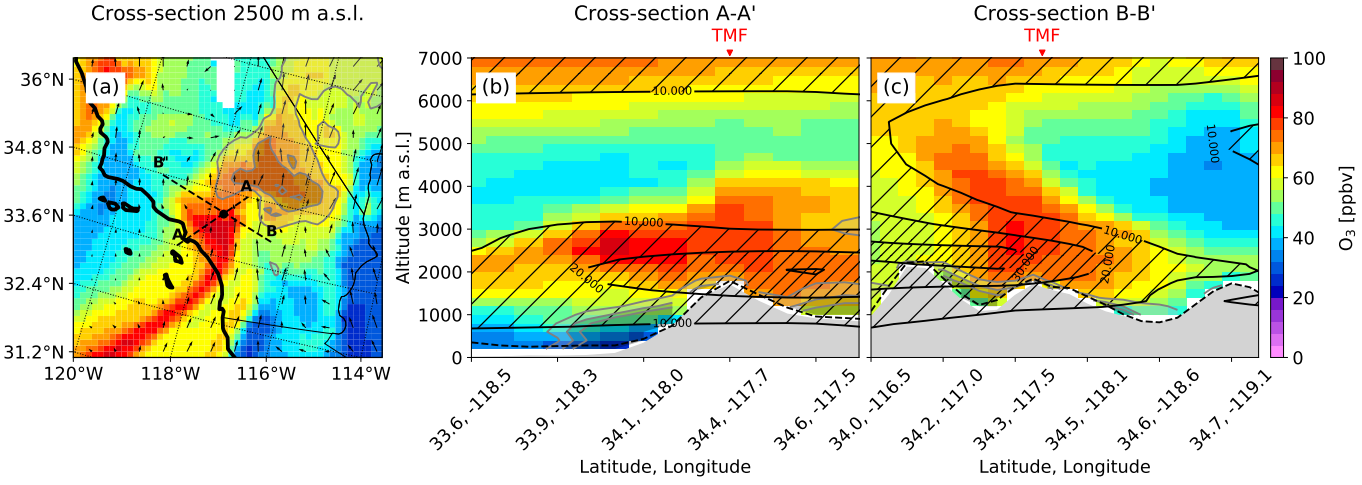

Figure 15. Horizontal and vertical cross-sections of WRF-Chem and WACCM forecast outputs for 3 July 6:00 UTC. Panel descriptions are the same as the ones shown for Fig. 12.

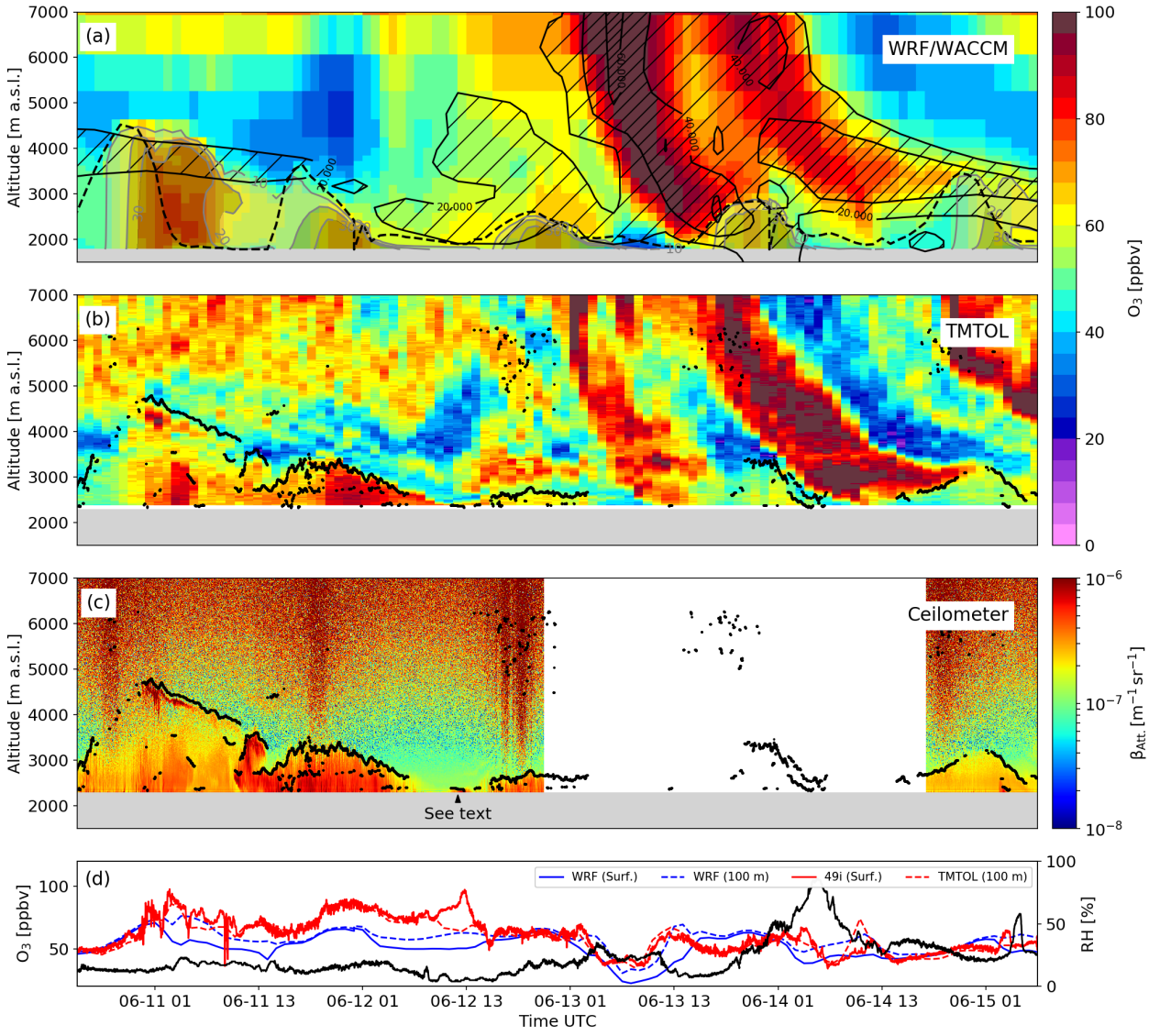

Figure 16. Overview of the model outputs and measurements over TMF between 10 June 15:20 and 15 June 7:10 UTC. Panel descriptions are the same as the ones shown for Fig. ~~13~~10.

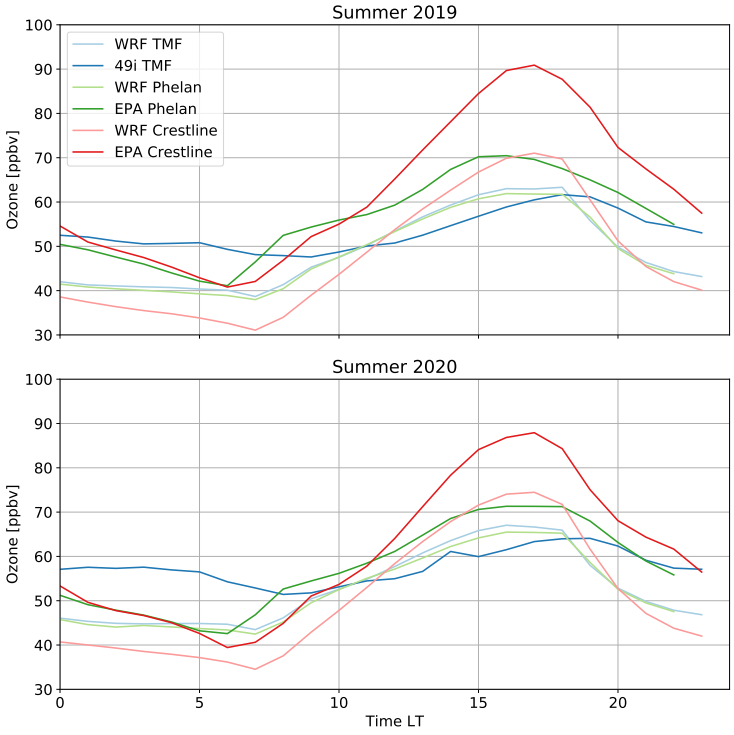

Figure A1. Mean ozone daily cycle at TMF and nearby stations (Phelan and Crestline) together with the corresponding WRF-Chem output for summer 2019 and summer 2020.

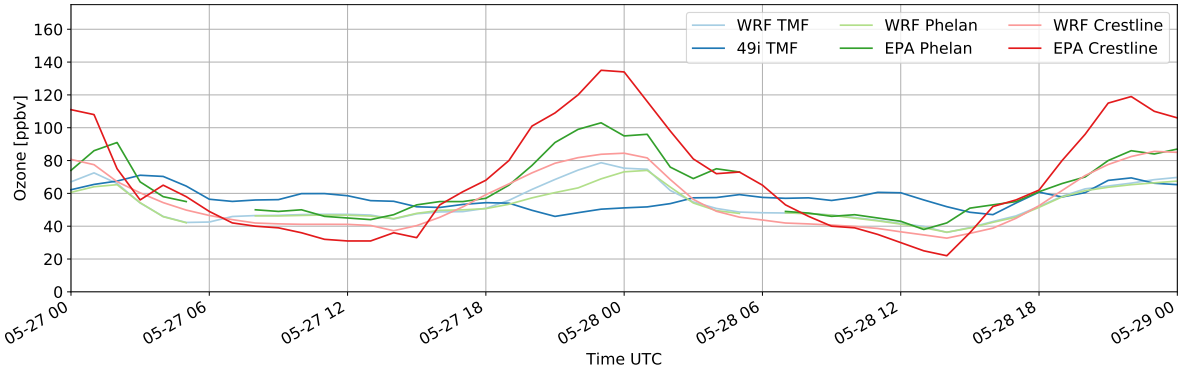

Figure A2. Forecast and measured surface ozone concentration at TMF and nearby stations (Phelan and Crestline) for the period comprehended between 27-28 May 2020.

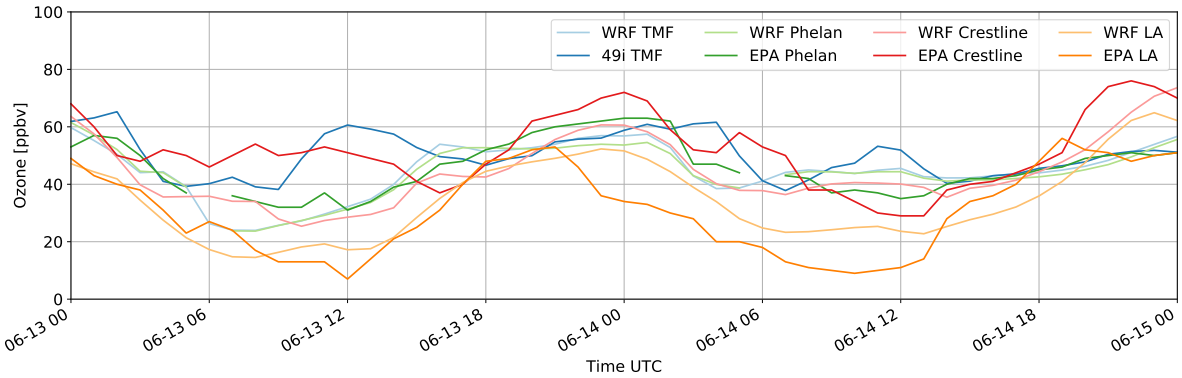

Figure A3. Forecast and measured surface ozone concentration at TMF and nearby stations (Phelan, Crestline and LA) for the period comprehended between 13-15 June 2020.